CORROSION PROTECTION WITH ULTRATHIN GRAPHENE COATINGS: A REVIEW

ANDRÁS GERGELY ✉ AND TAMÁS KRISTÓF

Department of Physical Chemistry, Institute of Chemistry, University of Pannonia, Egyetem u. 10.,
Veszprém 8200, HUNGARY
✉Email: gergelyandras@almos.uni-pannon.hu

Developments in surface treatment or finishing, and modification of structural metals have probably never been so dynamic than in recent years due to the need for new approaches to efficient corrosion protection. The application of coatings is a strategy to be followed to physically separate corrosive environments from metal surfaces. The overall protection efficiency depends on the coating's barrier properties. Traditional alternatives to coating suffer from inefficient physical protection in cases of low film thicknesses and at elevated temperatures. One of the most advanced options is to apply ultrathin atomic films to ensure complete separation of the metallic surface from the fluid media. Among the numerous materials and methods, exceptional chemical resistance and high domain size make graphene a promising candidate for constituting ultrathin coatings with interfacial atomic layers adherent and homogeneous coverage to feature firm barrier behaviour. This review focuses on the major efforts with notable results and points out some short comings that must be resolved to serve as a basis for further progress in this field.

Keywords: ultrathin coatings, graphene, metals, corrosion protection

Introduction

Nowadays graphene (Gr) is undoubtedly of great interest in many fields of science and engineering. The attention is due to its unique structure, electrical properties [1, 2], efficient heat spreading [3], wetting transparency [4], surface wetting tenability [5], and high reflectivity (mirrors for the beams of He and H_2) [6]. The Gr's practical impermeability to gases [7-9] is a result of the combination of its strong structure (carbon bond energy and intrinsic strength are 4.9 eV and 43 N m^{-1}, respectively) and its morphology that makes Gr to be the thinnest and most impermeable membrane [10]. In addition, because of its chemical inertness [11], especially against oxidation [12, 13], it is highly resistant to corrosion [14] under conditions where other substances would undergo chemical reactions [15, 16]. As a lightweight mono-atomic coating, Gr can function as one of the most advanced electron- and ion-transfer barriers at the metal-electrolyte interface, without notably altering optical properties and thermal conductivity of the substrates. Gr on metal surfaces is expected to afford oxidation resistance [11] based on its airtight balloon behaviour associated with its excellent barrier nature against oxygen diffusion [7]. Nevertheless, coherence, and uniformity of Gr coatings are apparently vital to achieve good corrosion protection. In accordance with general expectations, electrochemical properties of Gr [17, 18] and its coated derivatives were extensively investigated. The main results achieved recently are described in the following sections that are organised from the viewpoint of synthesis techniques and application purposes.

Pure Graphene Coatings

Direct Chemical Vapour Deposition (CVD) on Metal Surfaces

Early studies were inspired to synthesise full surface covering Gr films of the highest domain (single sheet) size and integrity to exert impermeability over macroscopically large surfaces. Later findings proved the viability of this concept as interfacial construction of thin layers is a promising way to provide durable corrosion protection for metallic substrates [19]. Generally, coatings play a vital role in improving surface quality and protection of substrates, since much effort has been made to produce films featuring excellent properties. Graphene is certainly one of the most prominent representatives of this kind and subsequently has been studied in almost all scientific and engineering fields. This new generation material has been a novel subject to incorporate into the latest corrosion protecting coatings. Achievements in utilising Gr as a pure and composite coating were first reviewed by TONG et al. [20]. The synthesis and functionalisation of Gr were briefly discussed and future perspectives suggested.

The simplest way is to grow Gr directly on metal surfaces, even though this strategy does not provide the most protective coatings due to low adherence of the inorganic layers as consequence of weak interaction. By direct CVD, metals like nickel [21], cobalt [22], iridium [23], ruthenium [24] and copper [21, 25-27] were coated with Gr (on large areas in certain cases) [25] using methane or acetylene as a carbon source [28, 29]. Deposition kinetics of carbon and the formation of Gr layers on copper were thoroughly explored; surface mediation theory was proved when poly-crystalline films were characterised with the domain size of 10 μm^2 [30]. Except for assessing the influence of grain orientation, the effect of other growth parameters was estimated. The most relevant findings are as follows:

1. The density of Gr nuclei decreased, conversely flake domain size increased as temperature increased and partial pressure of the carbon source decreased.
2. When the pressure dropped below a critical threshold then no Gr nucleation was observed and film formations terminated before reaching full surface coverage.
3. To achieve complete surface coverage, the partial pressure of methane must have been increased above 500 mTorr then full coverage was reached within 2 to 3 min. Only a supersaturated surface relaying on a critical threshold of partial pressure ~285 mTorr was suggested to drive the formation of fully coated copper substrates with a continuous layer of Gr flakes. Thus, carbon nuclei formed in the first step under a lower pressure followed by a second step of nuclei growth at a higher pressure, promoting full surface coverage.

The effects of these parameters coupled with the investigation of the orientation of metal crystals on Gr domain size were quantitatively evaluated at low temperatures [31]. The activation energy for Gr nucleation under atmospheric pressure was noticeably higher (9 eV) than under low-pressure CVD procedures (4 eV). Such a difference was attributed to copper sublimation at low pressure, because copper evaporation probably has a decisive impact on the desorption rate of carbon from the surface. Copper evaporation is restricted under atmospheric pressure, so the activation energy is assigned to the desorption of carbon clusters. Close to the melting point of copper, large single-crystal Gr synthesis was proposed at the highest possible temperature (probably to maintain the highest rate of interfacial mass-transfer, diffusion coefficient of the decomposed and fragmented precursor agents). By following these principles, single Gr crystals with a domain size of ~1 mm could be synthesised. The nucleation density was higher on (111) than on (100) and (101) surfaces without any identifiable preference at higher temperatures [32]. Under carefully optimised conditions, continuous films of some layers were obtained on polycrystalline nickel without void areas at the flake boundaries [21]. In that case, ambient pressure CVD was to grow Gr films of 1-12 layers, with flake sizes of up to 20 μm for single- and bilayers (BLs). An ultra high vacuum (UHV) chamber was not needed [33, 34] to finely balance nucleation and growth processes,

instead, thermal annealing was employed leading to the emergence of single-crystalline nickel with grain sizes of 1-20 μm. Grain surfaces became atomically flat with some terraces and steps similar to single-crystals usually used for epitaxial UHV experiments and Gr growth took place probably *via* the precipitation of carbon in the metal. Because metallic grains may independently affect film thickness as a result of the high density of atomic steps at grain boundaries, multi-layer (ML) nucleation occurred mainly at those areas.

By using atmospheric pressure CVD, high quality Gr was grown on copper, eliminating all the major difficulties associated with the low-pressure method. Parameter optimisation involved evaluating the influence of the thickness, purity, morphology and crystallographic orientation of the metal foils on growth rates and the number of Gr layers. Scanning electron microscopy (SEM) images illustrating Gr flakes on polished foils besides XRD patterns of annealed foils are presented in *Fig.1* showing large copper domains on NR foils. The effects of copper impurities on the density of bilayers are signified; complete surface coverage on AA2 (the purest foil (99.999%) without double layers), AA1 and NR. In *Fig.2*, Gr quality is presented at various distances along the tube reactor. The methane concentration was higher at the inlet leading to a greater abundance of MLs (darker islands in the images). Gradual increase of concentration resulted in the formation of single-layer (SL) Gr growth over the entire length. A constant methane concentration yielded a high percentage of MLs at the inlet, incomplete coverage in the middle and separated single domains (seen as darker islands) at the outlet.

As a method of surface pre-treatment, electro-polishing [36, 37] in phosphoric acid seemed to be a good choice to achieve an appropriate degree of surface cleaning and minimised roughness. Acetic acid was highly efficient at cleaning the copper surface, but only capable of removing oxidised species without any further etching. Etching with ferric chloride solution generally gave similar results to electropolishing despite the greater roughness of the $FeCl_3$ treated copper foils. This was probably due to the considerable scale of copper recrystallisation during annealing at temperatures close to the melting point of copper before the CVD process, leading to the evolution of a smoother surface with a low density of defects serving as nucleation sites. Additionally, the growth rate was estimated depending on the purity and crystallographic orientation of copper but by far not as much as the partial pressure of hydrogen, because the amount of dissolved hydrogen depends less on the thickness of the copper substrate. Crystallographic orientation was found to be an important factor, since the growth rate on the surface of substrates characterised by Miller indexes (100) was faster than on (111) surface under ambient pressure. In contrast, at low pressure and temperature the (111) surface facilitates the fastest growth rate [38]. Furthermore, optimal conditions to achieve full surface covering films with the minimum proportion of MLs might greatly vary with purity of the metal specimens. High purity substrates contribute to the formation of SL

Graphene Coverage vs. Copper surface orientation

Bilayer density vs. foil purity
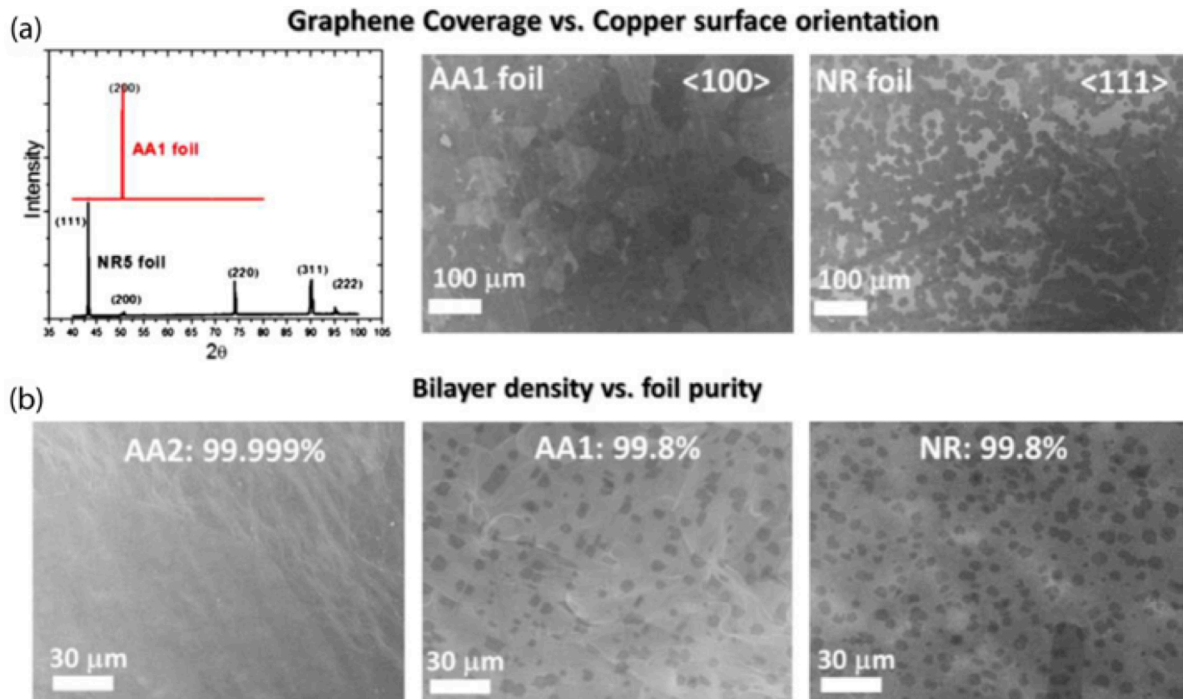
Figure 1: SEM images illustrate (a) Gr growth rate on polished AA1 and polished NR foils. XRD of annealed AA1 shows (100) orientation, the NR foil with the majority of (111) with smaller contributions from (110) and (311); (b) The effect of copper impurities on the density of bilayers [35] (republished by courtesy of the publisher, Elsevier)

films, and low purity metals support the evolution of multi-layer (ML) Gr coatings. Due to the multiple aspects of the reaction mechanism, optimal conditions for long foils are related to low and varied concentrations of carbon sources along the tube reactors, similarly to the application of temperature gradients (furnace dimensions and its relation to foil size) as well.
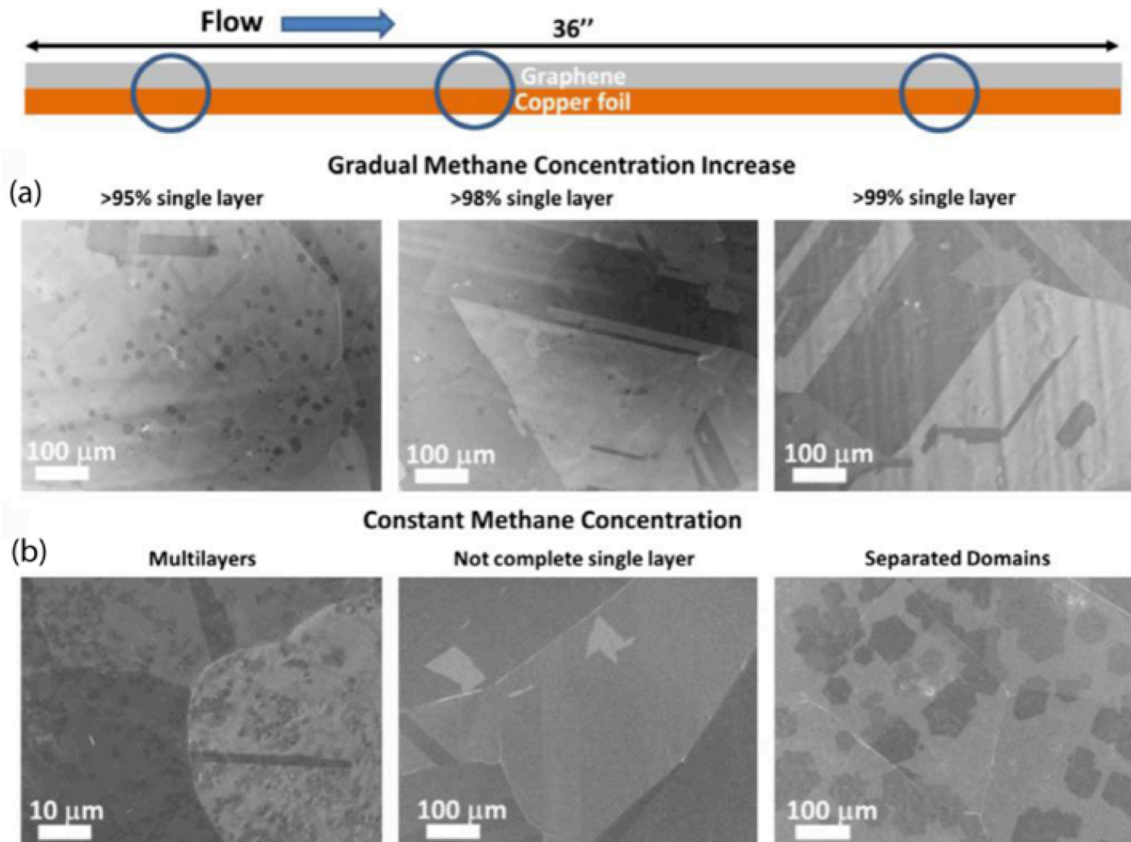
Figure 2: Gr films at various distances along the CVD reactor used at atmospheric pressure. (a) Gradual methane concentration, single-layer Gr growth over the tube reactor; (b) Multilayers at the inlet, incomplete surface coverage in the middle and separated single domains at the outlet [35] (republished by courtesy of the publisher, Elsevier)
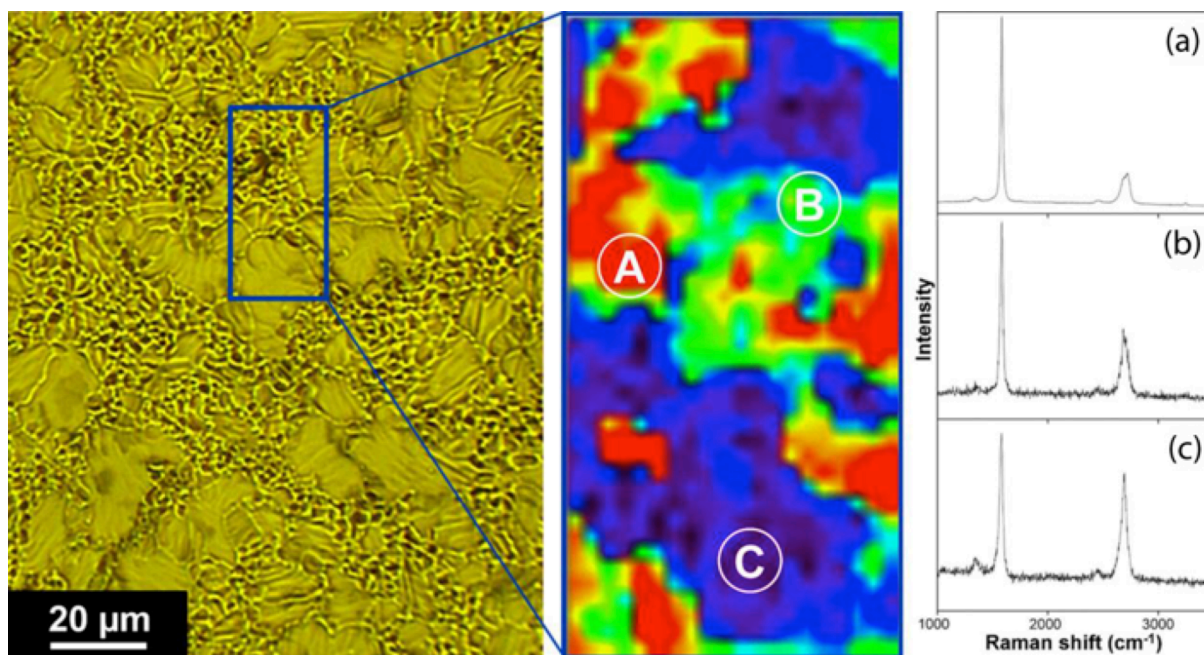
Figure 3: Optical micrograph, Raman map of ~2700 cm^{-1} peaks and respective Raman spectra of the areas on the Ni–Gr surface [41] (republished by courtesy of the publisher, Elsevier)

The gradual increase of methane concentration from 30 to 100 ppm in the mobile phase helps resolve the changing rate of activated carbon production [39]. Because methane concentration near the outlet increases slowly as a result of thermal decomposition and deposition, the main purpose of the gradually increasing methane concentration was to minimise bilayer growth at the inlet over the synthesis duration and to ensure full surface coverage near the outlet with the highest concentration of the carbon source. In fact, optimisation in the case of the atmospheric pressure CVD is more complicated than vacuum ones, which process in long tube chambers with small foils. A steady methane concentration at the inlet surely results in an increasing proportion of MLs at the inlet and incomplete coverage at the outlet, with visibly separated flake boundaries. The initial methane concentration of less than 30 ppm exclusively led to SL Gr at the inlet. High quality Gr grows with >99% monolayer coverage and in some cases films consisted of flake sizes of around 100 µm. High temperature etching with oxygen led to the visualisation of inter-domain boundaries as etching started at these boundaries and expanded into domains in a dendritic pattern, leaving diagonal stripes etch-free. Efficient corrosion resistive film properties were reported when experiments were made with samples exposed to air at 300 ºC, showing no sign of oxidation (oxygen enrichment in the metallic phase) over Gr coated areas in comparison to bare substrates.

According to a similar preference, growing Gr layers on copper is favourable, because copper does not dissolve carbon as much as nickel at high temperatures. However, it is also possible to grow MLs with highly ordered crystalline structures suing atmospheric CVD with controlled film thickness [40]. Both pure nickel and copper were covered with CVD grown Gr films detected as covering the majority of the metals in a SL form besides some areas of double and fragmented MLs

(less than 5% of the coating) [41]. An optical micrograph and Raman map with the respective Raman spectra obtained from the Ni–Gr and Cu–Gr surfaces are presented in *Figs.3* and *4*, respectively. Electrochemical tests indicated that such coatings substantially reduced the corrosion rate of the substrates. By Raman spectroscopy investigation, SL Gr showed sharp G (1580 cm^{-1}) and 2D (2650–2700 cm^{-1}) bands with a small G/2D ratio, whereas ML Gr with a high G/2D ratio and an altered, less sharp 2D band were detected. Hence, 80 and 60% of the copper/nickel surface was covered with Gr as a single- or few-layers coating without uniformity on nickel. Scanning electron micrographs of the samples showed different thicknesses of the films with various scales of folding, full of wrinkles and edges. Thus, the overall conclusion was reached that coherent SL Gr is hard to obtain by direct deposition processes. Immersion type corrosion tests indicated open circuit potentials (OCPs) or free corrosion potentials of copper and nickel shifted towards the positive potential region. The electrochemical test conditions are summarised in *Table 1*. A potential ennoblement of about 0.3 V was measured for the corroding system of nickel/Gr and a cathodic shift of ~0.2 V observed with coated copper samples. The cathodic reduction processes were affected, inhibited by the Gr layer on copper and the rate of anodic half-reactions was apparently reduced near the steady free corrosion potential. However, during extended linear potential scanning Gr/nickel showed higher anodic currents than uncoated substrates opposed to the modified copper that exhibited no changes in the anodic branch after Gr deposition.

As an oxidation barrier for liquid and liquid–vapour phase-change cooling systems almost the same heat transfer efficiency was reported using bare and Gr/copper surfaces in liquid-phase and two-phase thermal performance tests [42]. After thermal treatment,
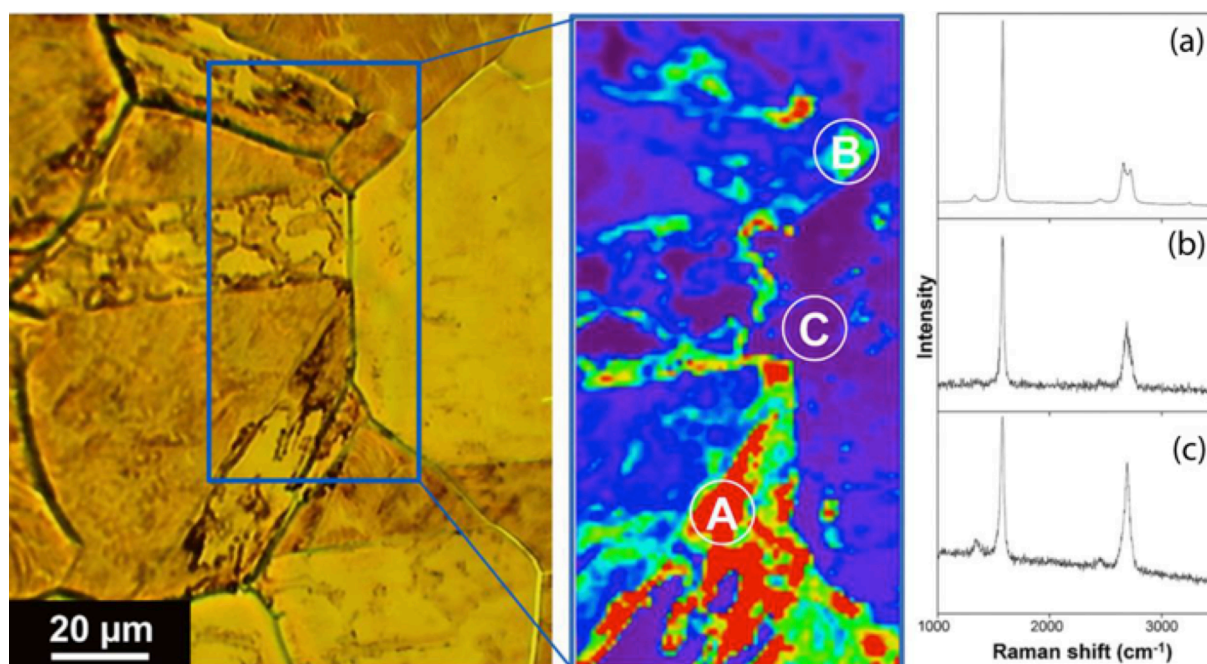
Figure 4: An optical micrograph, Raman map of ~2700 cm^{-1} peaks and respective Raman spectra of the areas on the Cu–Gr surface [41] (republished by courtesy of the publisher, Elsevier)

analysis revealed oxide formation on the entire surface of bare copper and limited oxidation at grain boundaries on the coated substrate. In conclusion, few Gr layers acted as a protective layer even under vigorous flow conditions near the boiling point of the fluid phase. Graphene prepared by microwave (MW) assisted CVD protected substrates from chemical oxidation when samples were heated under atmospheric conditions in a sequential multi-step procedure with dwelling times from 15, or 30 min to 1 h [43]. A very low degree of chemical oxidation of Gr over copper was indicated by XPS and the presence of cuprous oxide was found on the entire surface of bare specimens.

There are special applications such as steering and focusing elements for neutral atomic and molecular beams in de Broglie microscopes [44]. These mirrors utilise the quantum reflection of an atomic beam on metal surfaces since interaction volume is strictly limited to an extremely thin atomic layer of the metals. Oxidation and any other form of corrosion or adsorption of atmospheric gases might well lead to far lower reflectivity of the metallic surfaces, and the coatings of more than a few atomic layers are unacceptable. Thus, there are exceptional requirements of protective coatings and Gr films were expected to provide the solution in this matter too. Complete and uniform monolayers could be grown on polycrystalline ruthenium of a columnar structure on fused silica, exposing flat surface facets [45]. Single-layer Gr protects underlying metals with special structures like concave focusing mirrors and non-planar micro-electrode arrays from oxidation under ambient gases. Ruthenium was recovered by heating the samples under ambient conditions at 250 ºC for half an hour in an ultra-high vacuum, which was indicated by missing peaks in the oxygen (1s) region of the XPS spectra.

Gr on copper provided mediocre protection against electrochemical degradation in chloride environments [46]. Impedance measurements showed increased resistance at the metal/solution interface as anodic and cathodic current densities decreased with about hundred times higher charge-transfer resistance besides about thousand times lower double-layer capacitance in comparison to uncoated copper. Ennoblement of the free corrosion potential was also observed and related to the good barrier nature of the film.

The protection of copper against corrosion by the growing number of Gr layers was in part demonstrated [47]. To enable reliable and complete mechanical blockage by the coating exploiting its impermeability and chemical inertness, preparation parameters were balanced to obtain an appropriate film structure. In *Fig.5*, cyclic voltammograms (CVs) of the bare and passivated copper (the latter with 1-3 Gr layers) are shown along with the intensity of oxidative currents besides the atomic force microscope image of the Cu/Gr after etching.

Fig.6 depicts CVs of Gr-coated copper and Gr-copper post-treated with aluminium oxide (AlO$_x$) of different thicknesses, along with the comparison of their peak currents. Nonetheless, nanometre size structural defects at flake boundaries were the main source of deficiency, decisive in the often-observed limited protection efficacy. To circumvent this problem, a general strategy is to grow ML island-free Gr films. Selective coverage of defect areas was achieved by atomic layer deposition, resulting in enhanced protection of ~99%. Bare copper in an aerated sulphate solution indicated a pitting corrosion rate of ~9 nm s^{-1} with a density of ~1 µm^{-2}.

The estimated diffusion rate of the reactants was above 1 m s^{-1} limiting the rate of corrosion processes.

Table 1: Metallic substrate, type and growth parameters to obtain Gr films by direct CVD deposition

Substrate	Preparation type & parameters	Corrosion test parameters	Surface of the working electrode (cm^2)	Types of electrochemical test	Ref.
Cu & Ni	CVD grown on metal surfaces	flat-cell, 0.1 M NaCl	0.07	potentiodyn. pol., scan rate: 1 mV s^{-1}, after min at OCP	[41]
Cu	CVD grown	flow-cell, mass velocity: 38 kg m^{-2} s^{-1} for 9 h, T = 59.5±0.5^{o}C	3.06	none	[42]
Cu	MW assisted CVD	heating at 150°C, in air at 1 atm for 1 h	Unknown	none	[43]
Ru	CVD	ambient exposure	Unknown	none	[45]
Cu	CVD	0.1 M NaCl	0.785	potentiodyn. pol., scan rate: 0.5 mV s^{-1} from OCP, EIS after 1 h	[46]
Cu	CVD	aerated 0.1 M Na$_2$SO$_4$	0.24	cyclic voltammetry, scan rate: 10 mV s^{-1}	[47]
Ni	CVD	treated at 600 ^{o}C in air, then 31 wt.% H$_2$O$_2$ for up to 2 h	Unknown	none	[49]
Cu & Ni	CVD & mech. transferred by spin-coating with PMMA at 4000 rpm for 45 s	0.1 M NaSO$_4$	0.4	potentiodyn. pol. & CV, scan rate: 0.005 mV s^{-1}, EIS	[50]
Cu & Si	CVD then transfer of layers with PMMA cured at 165 ^{o}C	ox. at 225 ^{o}C for 60 min and red. of Cu at 450 ^{o}C for 90 min under O$_2$ and H$_2$ flow	Unknown	none	[60]
Cu	CVD, thiol func.: SLG-Cu treated with HCl & H$_2$O then 7.5 mM thiol-ethanol treatment for 2 h	lymphocyte transformation test & *in vivo* experiment	1.4	tests: Cu conc. by ICP-OES, cell viability & stimulation index for lymphocyte	[80]
Ni	template directed CVD	anode in glucose based electrolyte, Ni in ferricyanide catholyte	8	CV and EIS	[116]

Interestingly, in the case of the ML Gr films, mass transport remained fast across the sheets and parallel along their planes, which was anticipated by the outcome of a water permeation experiment [8]. This may explain the unchanged chemical inertness of the Gr coating, owing to the fast mass transport along and across the layers as etchant species permeate through unburied areas in outer layers and diffuse laterally while finding open areas in layers underneath. Inertness to electrochemical reactions could only be attained by thin layer deposition of aluminium oxide (within ~5 nm) by the means of an atomic layer deposition technique on Gr/copper. Only by this way could unburied regions on the copper surface be made void-free. After 160 atomic layer deposition cycles with a ~16 nm thick passivating film inhibition efficiency was ~99%. This was partly confirmed by Tafel analysis giving instantaneous general corrosion rates of ~99% to the copper-single layer Gr with 16 nm aluminium oxide and 87% to SL Gr/Cu, in comparison with bare copper.

The approach of the direct loading of a precursor, i.e., acetone on copper then annealing it to convert its vapours into Gr was investigated [47]. Monolayers formed with nearly 100% coverage after rapid thermal annealing. Under optimal conditions, acetone derived films with good crystallinity compared to common CVD grown counterparts. The passivity of the metal coated/masked with SL Gr was attributed to remarkably

inhibited cathodic reduction reactions and barrier action against the diffusion of anions accessing the underlying substrate. So, SL Gr/copper exhibited ca. forty times lower corrosion rates compared to the mechanically polished copper, which means an inhibition efficacy of up to 97%. Nevertheless, optimal protection performance was proposed to be achieved by the application of four Gr layers with their short-term inhibitions of up to 99%. The corrosion current of the Gr/copper reduced by ca. sixty times compared to mechanically polished substrates and the OCP shifted towards the negative potential region. Electrochemical impedance spectroscopy (EIS) indicated ten thousand times lower electrolyte-metal interfacial capacitance (C_{dl}) of the Gr/copper samples than those of the mechanically polished specimens. Such a notable drop suggests a significant shrinkage of the exposed surface to the electrolyte. C_{dl} of the Gr/copper was ca. three times higher in NaCl solution (0.6 M) than in its diluted media (0.1 M), but 6.4 times lower than that obtained in 0.1 M Na$_2$SO$_4$. C_{dl} and constant phase element (CPE) of the Gr/copper samples suggest an electrochemically smaller active surface to interfacial charging (discharging) and adsorption (like a non-Faradaic Helmholtz capacitor) as the density of conductive pathways decreases besides the lower effective surface roughness than that of the mechanically polished substrate. The CPE was 2.7 times higher than that
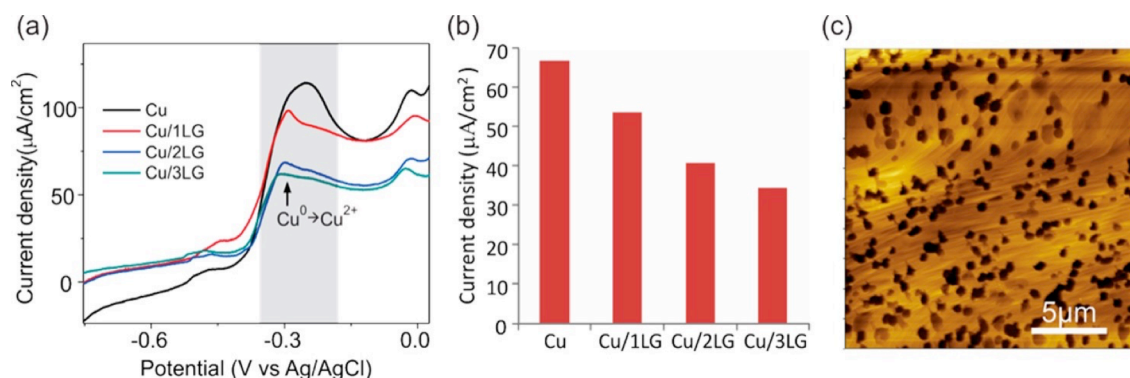
Figure 5: CVs of (a) bare Cu and Cu passivated by 1-3 layers of Gr, (b) intensity of oxidation currents under various passivation conditions, (c) atomic force microscope image of Cu/Gr after etching (adapted with permission from Ref. [47] Copyright (2014) American Chemical Society)
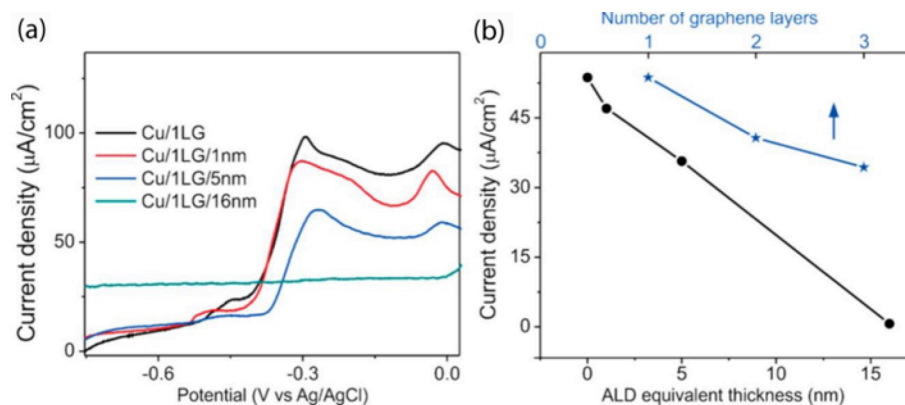
Figure 6: CVs of (a) Cu/Gr/Al samples, (b) Peak currents of Cu(0) for Cu/Gr/Al with different aluminium thicknesses and in comparison to Cu/Gr with 1-3 Gr layers (adapted with permission from Ref. [47] Copyright (2014) American Chemical Society)

measured in NaCl solution (0.1 M) and over ten times lower than in Na_2SO_4 solution (0.1 M). The resistance of coated copper to corrosion (R_{corr}) was ca. thirty five times higher than those of mechanically polished ones 6×10^4 and 1.6×10^3 Ω cm^2, respectively. R_{corr} was appreciably lower than that of NaCl and higher than with Na_2SO_4 solutions. Thus, inhibition efficacy was found as follows; >97% in 0.6 M and >71% in 0.1 M NaCl. Thus, performance was sensitive to the integrity of the Gr film as mechanically polished samples indicated rapid protection efficiency losses with increasing chloride concentrations in the test solutions.

Rigorous corrosion testing of nickel/CVD grown Gr films revealed low intensity oxidation of the substrate by heat treatment. Oxidation resistance was effective up to 500 ºC for 3 h, and with durable exposure (2 h) to essential hydrogen peroxide (31 wt.%) solution [49].

Both nickel and copper were coated with ML Gr films [14] by mechanical transfer. CV measurements indicated a remarkable restriction of the evolution of anodic and cathodic current transients, resulting in the effectively decreased electrochemical activity of the metal substrates. *Fig.7* depicts CVs of bare and Gr-coated copper samples, and XPS spectra of copper under ambient conditions, at 100 mV and sputter cleaning. Region (i) and (ii) contains a shoulder and a peak due to CuO and Cu_2O/Cu, respectively. The third part of the figure shows SEM images of Cu and Gr/Cu before and after voltammetry scans. Based on Tafel analysis, corrosion rate assessment (quantification prediction) for bare substrates gave the following results: ca. 6×10^{-13} and ca. 3×10^{-14} m s^{-1} for copper and nickel respectively. Graphene/copper indicated lower corrosion rate of ca. 8×10^{-14} m s^{-1} up to ca. seven times less than the bare substrate. The Gr/nickel showed a reduced rate of ca. twenty times to 2×10^{-15} m s^{-1}. With two or four folds of Gr layers, the corrosion rate of nickel decreased to 2×10^{-14} and 8×10^{-15} m s^{-1} respectively, which is considered as a notable performance improvement.

EIS measurements suggested an undamaged state of Gr, but the metal surface might corrode at high rates around void areas in the film. The most probable electrical network included resistive elements of the solution; $R_s \approx 40$ (6.5 Ω cm^2) and charge-transfer at the interface; initial $R_{ct} \approx 3\pm0.5$ kΩ cm^2 due to Faradaic processes. The mass transport process was modelled with a Warburg element ($W \approx 1.0\pm10^{-3}$ Ω^{-1} s$^{0.5}$ cm^{-2}) as a semi-infinite diffusion component. The inhomogeneity of the surface was handled by incorporating a CPE as a non-ideal capacitance in the circuit due to the impedance dispersity of the electrical double layer component at the metal-liquid interface. Double layer capacitance was best achieved with 2.2 μF cm^{-2} and the CPE was $Y_o \approx 7.6\pm10^{-5}$ Ω^{-1} s cm^{-2}. Increased resistance coupled in series was caused by the electrical surface resistance of Gr ($\approx$1 kΩ) with a double layer capacitance of ~3.8 cm^{-2}. Average fitting parameters were changed
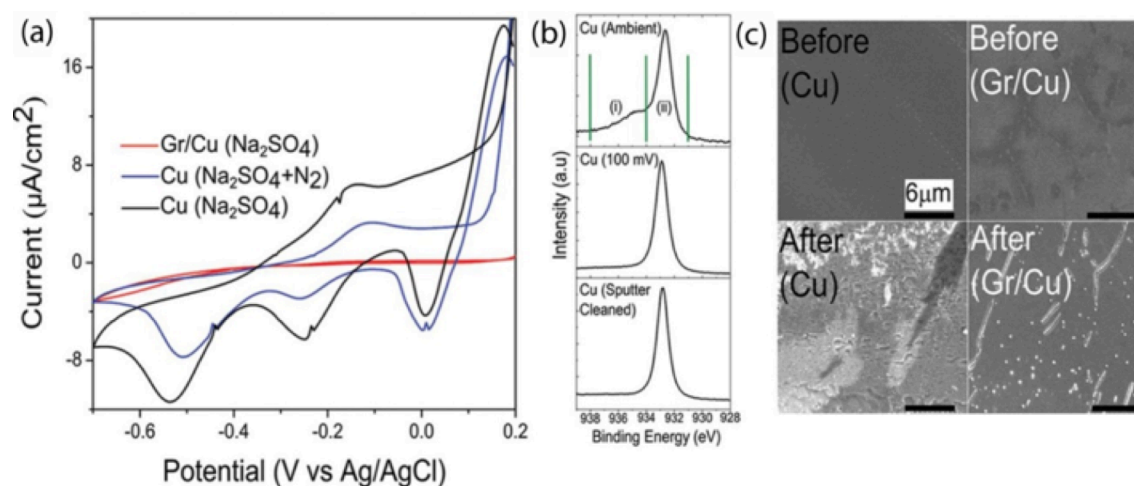
Figure 7: CVs of (a) bare Cu and Gr/Cu samples with the blue line corresponds to the measurement with N_2 bubbled through the solution; (b) XPS spectra of copper under ambient conditions at 100 mV and sputter cleaning with regions (i) and (ii) are due to CuO and Cu_2O/Cu(0), respectively; (c) SEM images of Cu and Gr/Cu before and after CV scan (adapted with permission from Ref. [14] Copyright (2014) American Chemical Society)

accordingly as follows: $C_{dl} \approx 9\pm5.0\ \mu F\ cm^{-2}$, CPE: $Y_o \approx 2\times10^{-5}\ \Omega^{-1}\ s\ cm^{-2}$, $W \approx 3\pm0.5\ \Omega^{-1}\ s^{0.5}\ cm^{-2}$, and $R_{ct} \approx 10\pm1.2\ k\Omega\ cm^{-2}$. The C_{dl} was ca. ten times lower than measured with bare copper, which seemed to be unrealistic. Such a difference is thought to originate from the quantum capacitance of the Gr film as a contribution in series with the C_{dl}. This is partly due to the small density of states in the Gr, which is in good agreement with the reported quantum capacitance of 7–10 $\mu F\ cm^{-2}$ [50]. The increased R_{ct} of the copper samples in comparison with the one measured at the beginning of corrosion test suggested that the minor proportion of the metal substrate was uncoated with Gr, participated in corrosion processes. The proportion of this unburied area was estimated to be unexpectedly high ($A \approx 0.3$), exceeding the scale impressed by microscopy images ($A < 0.05$). Such a difference was attributed to the access to larger substrate areas by the diffusing depolarisator species and a subsequent greater proportion of Helmholtz capacitance then pseudo-capacitance based on electrochemical activation of metallic substrates for anodic reactions.

Nevertheless, the ability of Gr to catalyse, and depolarise cathodic reactions such as oxygen reduction [51] by well-coupling micro-galvanic cells in contact with the poly-aromatic sheets [52] either in planar or concentric forms (according to the function of the surface quinone group on carbon electrodes, i.e. GARTEN and WEISS's mechanism) is almost always a concern. Thus, protection efficiency depends largely on the deposition technique, quality, and epitaxial pile structure of the Gr sheets, affecting ionic and electrical transport through the films. Due to low adherence as a result of the lack of direct grafting or anchoring type chemisorption, direct CVD-grown films are classified as fragile coatings liable for potential polarisation and charging of the surface due to their structural alterations [53]. To increase the small domain size of the flakes, high temperature annealing at ~1035 ºC on the metal surface offers a resolution promoting further development of coherency of the films composed of large domains [54]. However, there are many

problems with direct CVD deposition on metals like nickel because of the film formation mechanism of polyaromatic carbon materials.

The mechanisms of surface catalysis and adsorption during Gr growth on copper were determined [13, 55] to be different from film growth on nickel, which is governed by the combination of catalysis and adsorption as well as solubility and rejection. As the CVD technique enables the synthesis of Gr on larger metal surfaces [22, 56], carbon sources are thermally decomposed and fragmented into smaller segments, then atoms arrange into 2D honeycomb lattices. The preparation of CVD grown Gr films takes place readily on surfaces with face-centred cubic and hexagonal close-packed crystal structures. Methane and ethylene, which decompose at a temperature of ~1000 ºC are used as main precursors [24, 25] even though such a high temperature might significantly affect the metallographic state of the substrate, nucleation and deposition kinetics. Metals with close to zero solubility of carbon at the reaction temperature, e.g., copper, deposit *via* a catalytic mechanism and they are more likely to assist the formation of SL Gr instead of ML ones owing to the lack of catalytic effect after the first layer is deposited. Thus, the metal surface acts as a catalyst facilitating Gr growth in the form of a finishing coating, as deposition is restricted to SL [57]. Film growth on metals with mediocre carbon solubility at reaction temperatures undergoes *via* a complicated mechanism in which carbon diffuses into the bulk metal, e.g., nickel, and is rejected during the cooling process because of the decreasing solubility at lower temperatures. The rate of carbon rejection is critical to the development of ML Gr coatings. Hence, these films form preferentially instead of SLs on copper. Further complications may arise by the use of thicker metal specimens because thicker substrates dissolve larger amounts of carbon during the cooling phase since they release more carbon to produce larger amounts of carbon soot. Although any process that needs to be scaled-up must be optimised for engineering alloys, there are many results of theoretical interests as well.

A thesis [58] thoroughly investigated the protection efficacy of direct CVD grown Gr on copper, depending on flake size and uniformity, duration and temperature of the heat treatment. Key factors leading to firm protection performance both in terms of instantaneous and long-term functions are identified as to eliminate defects in the Gr sheets, flakes must build up a flawlessly continuous, coherent, and uniform film. Low nucleation and high growth rates must be maintained under low pressure to gain a low density of carbon spots (as probability of deposition decreases) and coherent films with the absence of unburied areas at flake boundaries. The films with large flake sizes were tested in a number of experiments to optimise growth parameters in order to reduce the amount of disorders, defects and void areas. A series of chemical oxidation experiments were performed by heating bare and coated copper foils at various temperatures and for various time frames. Ellipsometry helped characterise the thickness of oxide layers on the highly reflective copper. Heat treatment was carried out at 120 ºC under air for up to 76.5 hours. The growth rate of copper oxide layers, as an inherent indicator of the oxidation rate, almost linearly increased with time and the difference was only ca. a factor of six between the bare and coated copper foils. Corrosion deterioration was located at two spots where air leaked through defects in the Gr film and around its flake boundaries. Following growth time in low pressure CVD experiments, films were grown in a way that their flakes were not connected. Therefore, flake growth stopped before expanding sufficiently to connect with one another. Then oxidation was performed at 190 ºC for up to 37 h and 26 min. Optical microscopy images revealed a remarkable difference between the bare and coated copper samples. Then oxidation was repeated with closely spaced Gr flakes investigated by optical and SEM. The samples with closely spaced flakes gave very good results after a 30 min treatment at 190 ºC. A 13.5 h treatment led to minor deterioration in the substrate exhibiting black oxide patches on the surface but a 23 h and 35 min annealing resulted in corrosion of nearly the entire surface.

In a series of experiments, copper substrates coated with continuous Gr flakes were treated at 190 ºC for various periods of time. After a 30 min heating, samples exhibited a fine condition with some proportion of the surface composed of dark copper oxide. After a 10 h and 45 min treatment, migration of the corrosion front on the copper surface (CuO formation) proved to be far advancing and the heavily corroded areas showed a homogeneous distribution in the form of tree roots. Optical microscope images after 35 hours of heating indicated heavy corrosion, but the surface was not fully covered with oxides. Raman spectroscopy quantitatively characterised copper oxidation, which could proceed at flake boundaries as they feature the least hindrance to mass transport of depolarisators and the large sheets did not damage or etch oxidatively inside.

Apart from growth related issues, electrochemical aspects of the shortfalls may also be relevant. Gr films, acting as physical separators, might take part in electron transport, helping interfacial charge-transfer perpendicular to the surface based on good coupling and ballistic electron transport parallel to the basal plane of the sheets. Oxygen adsorption and reduction reactions with low activation energies may further complicate the application of this material, which has been recently underlined in a short- and long-term performance test of Gr/Cu and Si substrates [59]. Results clarified that the samples heated at 250 ºC for 6 min showed heavy oxidised spots on bare copper, but little oxidation on the Gr coated one. Therefore, Gr served as a sufficient oxidation barrier helping to preserve the metallic state from chemical oxidation over a short time period at high temperatures. Nonetheless, long-term annealing of coated copper led to severe oxidation probably because oxygen diffusion proceeded through discontinuities and defects around Gr sheets. After 17 h at 250 ºC, coated copper became heavily oxidised in a way indistinguishable from the bare specimens subjected to the same conditions. Similarly, a 15 min treatment at 185 ºC resulted in partial oxidisation of bare copper but coated samples remained almost entirely in a pristine state. Nevertheless, after 17 h annealing in air at 185 ºC, both bare and monolayer coated substrates became severely corroded and the products were identified as cupric oxide (CuO) in a stoichiometric ratio. The timescale of protection against thermal oxidation by Gr on copper was estimated to be ~1 h at 185 ^{o}C and ca. ten times faster at 250 ºC. To explore the long-term protection ability under less severe conditions, bare and coated copper specimens were stored under ambient conditions (at 25 ºC) at low but variable humidity levels for up to two years. Bare copper showed relatively slow oxidation at room temperature. Gr/Cu tested after up to eighteen months exhibited oxide-free condition over the first two weeks but within a month the surface started to tarnish non-uniformly (in several hundreds of micrometres in size). Within a few months, most of the regions became heavily oxidised with an estimated oxide layer thickness of tens or hundreds of nanometres. Alignment between the substrate grains and Gr flakes was concluded to have an influence on oxygen and water diffusion along the surface. After eighteen months, the entire surface had become oxidised as EDAX analysis revealed a predominant percentage of cuprous oxide (Cu_2O) in the oxide phase. Gr/silicon gave similar results as bare and coated samples were compared to each other after one week under atmospheric conditions, indicating an increased oxygen content of silicon as time of exposure increased. According to the outcome of the series of experiments, short-term oxidation testing reflected some degree of protection but long-term propagation unveiled extensive wet corrosion, similar to that seen in the case of bare copper specimens. The high rate of the wet corrosion of copper is due to promoted galvanic cell formation on a micrometre scale at ambient temperature, especially over long-term exposure.

As a special field, the majority of medical applications require metals even today, in bone and joint replacements [60, 61], stents [62, 63] dental materials [64, 65], pacemakers and generators [66, 67]. Stainless
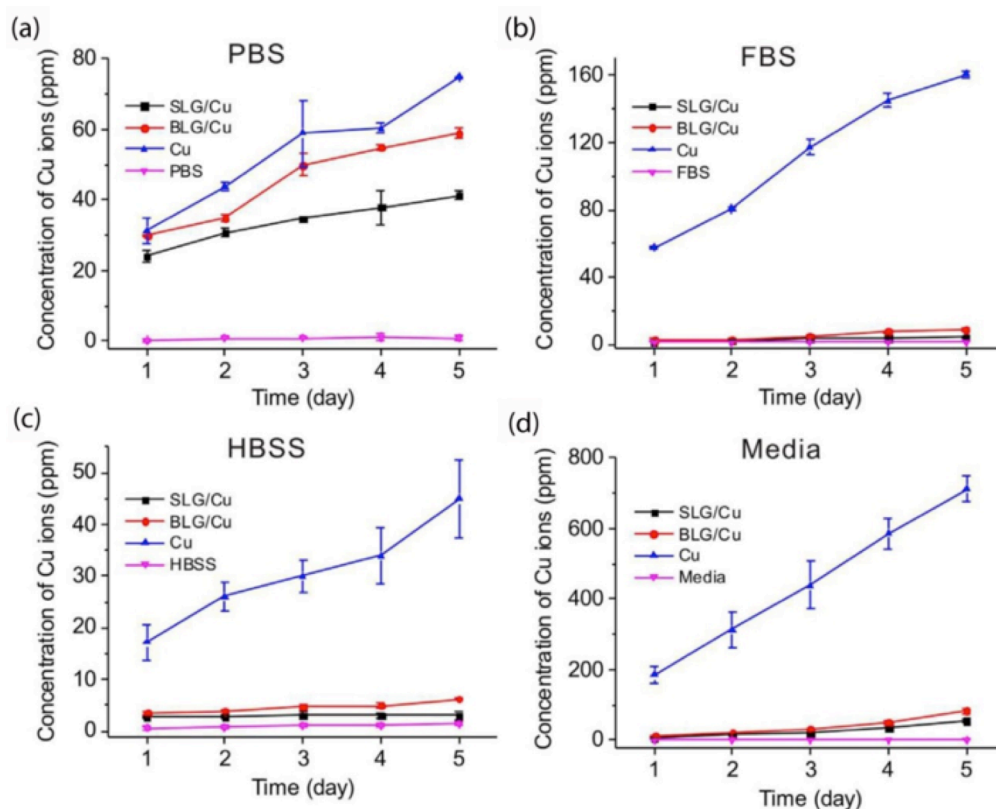
Figure 8: Concentration of Cu(II) ions from different biological solutions: in (a) PBS, (b) FBS, (c) HBSS solutions, and (d) cell culture media in the presence of SL (black) and BL Gr/Cu (red), Cu (blue) and blank solutions as controls (pink) measured by inductively coupled plasma-mass spectrometry (ICP-MS). All results are presented in a mass ratio (ppm) [79] (republished by courtesy of the publisher, Nature Publishing Group)

steel, titanium and cobalt alloys are the most common orthopaedic materials for joint prostheses articulated with a plastic bearing surface for many body parts [68, 69]. There are areas that require the use of alloys of mercury, silver, tin, copper along with limited amounts of zinc, palladium, indium, selenium and titanium in dental surgery [70, 71]. Despite the numerous successes, the main disadvantage of most of the alloys in medicine is their corrosion and the resulting physical deterioration (disintegration), quantity loss and contingent toxic side effects. The increased concentration of the aforementioned elements as soluble metals surely leads to chemical reactions of altered enzyme functions. It has been proven that soluble metals released because of corrosion processes can induce an innate monocytes-macrophage response and trigger immune responses, causing toxic, inflammatory, allergic or mutagenic reactions to patients [72]. In addition, corrosion leads to the adverse formation of metallic debris; solid particles and inorganic or organometallic compounds, in the periprosthetic soft tissues causing metallosis [73]. Furthermore, the corrosion degraded structural integrity leads to the premature failure and loosening of the metal devices [74]. Therefore, corrosion protection of metals used in physiological environments is of paramount importance and needs to be properly addressed for the sake of durable successful biomedical applications. Currently ceramic coatings are the most widely used to isolate metals from body fluids, e.g., zirconia transited from a zirconium alloy minimises corrosion in knee

implants but the implants roughen with time. Nano-size diamond coatings and apatite-nano-diamond composites are promising candidates for the protection of metallic implants [75, 76], but they are highly permeable and greater surface roughness notably decreases their performance. Nowadays, atomic thin Gr films enhance the bio- and hemo-compatibility of implants to some extent [77, 78]. Interestingly, the outcome of almost all cell viability tests showed the biocompatibility of Gr on the nickel-titanium surface with some protection. After considering these facts, studies focused on clarifying the possibility of application of Gr as a corrosion protective film on structural metals used for biomedical devices. The most important future application would be the efficient corrosion protection of metallic prosthetics to avoid serious health problems to patients. In an effort to offer an alternative to protect metallic implants, Gr was proposed as a biocompatible and protective film as well [79]. Copper was the substrate for cell viability tests to reveal any change in immune response (lymphocyte transformation test) and the metal sensitivity test because of its high toxicity [80] making the experiment sensitive to reflect any significant protection. In vivo experiments served to study the protection of copper in live animals to evaluate Gr as a biocompatible film in physiological conditions. Corrosion inhibition of copper with Gr films was studied by the way of release and accumulation of copper ions in biological aqueous environments of phosphate buffered saline, fatal bovine serum and Hank's balanced salt solution. Cell culture
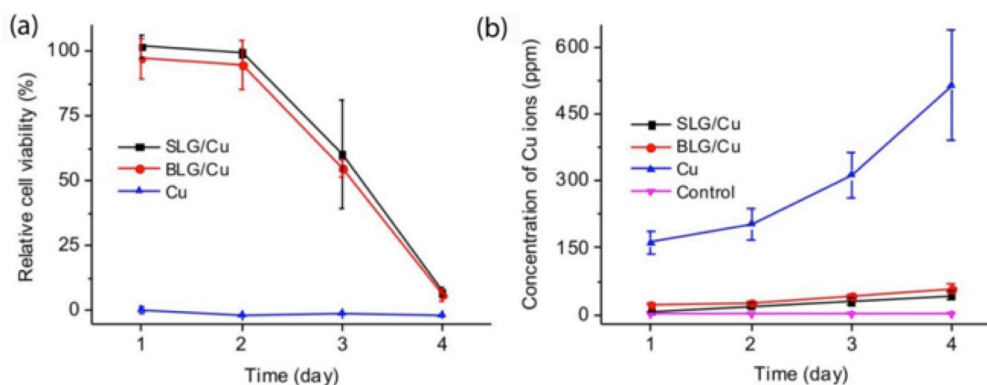
Figure 9: Relative cell viability and concentration of Cu(II) ions as a function of time. (a) Relative cell viability vs. time for SLG/Cu, BLG/Cu and Cu; (b) Concentration of Cu(II) ions in the cell culture medium after incubation with SLG/Cu. BLG/Cu and Cu (calculated from ICP-MS). A medium taken from a regular cell culture without Cu foils was used as the control [79] (republished by courtesy of the publisher, Nature Publishing Group)

media were monitored with inductively coupled plasma optical emission spectroscopy (ICP-OES) for five days. Single-layer Gr/copper indicated slightly varied but very good conditions on average.

The copper ion release rate was found to be at least an order of magnitude lower compared to bare copper that correlates almost linearly with time. The copper concentration in the solutions was higher when bilayer Gr/specimens propagated as compared to those of the tests with SL Gr obtained in all solutions. This was attributed to the stronger adhesion of SL films to metallic surfaces than bilayer ones, probably because of the better adaption to surface topography with high flexibility [81]. *Fig.8* shows the concentration of copper ions detected in different biological solutions such as phosphate buffered saline (PBS), fetal bovine serum (FBS), Hank's balanced salt solution (HBSS) and cell culture media with SL and BL Gr films and blank solutions as controls. Cell viability tests indicated almost the same results with single- and bilayer Gr/copper samples showing ±2.2 and 2.6% differences respectively compared to the control samples after the first day. Nonetheless, the results produced by low concentrations of dissolved copper in test solutions do not mean good results overall because the ion concentration could be much higher in a micro-milieu between the cells and coated substrate. The point of such a difference can explain why the cell viability dropped remarkably by more than 90% over the second, third, and fourth days of the test compared to the Gr contained samples although the copper concentration in the solutions remained very low (less than 70 ppm). Probably interfacial accumulation of metal ions must play a pivotal role in exceeding the toxicity limit, inevitably triggering lower cell viability. To resolve this problem, a further modification of the metal surface was necessary [82, 83]. By self-assembly monolayer treatment with decanethiol, bare and Gr/copper was modified with decanethiol, which was obviously assembled on the bare surface around the boundaries of Gr flakes. This is because the seemingly proper protection of copper was accompanied by much improved cell viability over three days *(Fig.9)*. The thiol modified SL Gr/Cu indicated that cell viability was ca.

55.8% after an incubation period of three days compared to SL Gr/Cu *(Fig.10)*. Thiol modified copper showed an improvement of up to 2% in comparison to the less than 1% viability observed for bare copper. These results suggest that Gr on copper is the major factor for protection, which can be appropriately enhanced by thiol modification. The film was also found to reduce immune response to copper in a clinical setting by a lymphocyte transformation test.

Animal experiments indicated a positive outcome to coated copper samples tested under *in vivo* conditions. The copper concentration was less than 3 and ~4.5 ppm in blood samples extracted from living rats implanted with SL coated and bare foils, reflecting the potential of thin Gr films in biomedical applications.

CVD-Grown Graphene Loading on Metal Surfaces by Mechanical and Electrical Techniques

Spin-Coating

There are a number of techniques to obtain high quality thin films. Static and dynamic dispense techniques such as dip [84-86], angle-dependent dip [87, 88], and hot dip spin, spin [89-92], spray [93], flow [94, 95], capillary [96, 97], roll [98], and reverse roll coating [99, 100] have developed thin layers on solid surfaces. By careful design, it is also possible to complement one another, offering a way to be tailored to application demands. Optimisation of these techniques is mostly dependent on actual parameters of the fluid phases and molecular or colloid solutions such as concentration, temperature, pressure, partial pressure or volatility of substances and solvents, dynamic or kinetic viscosity, and surface tension of fluid phases. The texture (roughness) of the substrate surface has much less influence (except for the surface energy) on the quality and quantity of casting. Drying and curing might later take place. From them, the ones featuring well controllable Gr growth are detailed in the following. Both spin-coating (SC) and kinetic spray (KS) are relatively novel techniques enabling us to form coatings of good quality on any sort of surface texture regardless of the substrates. SC is
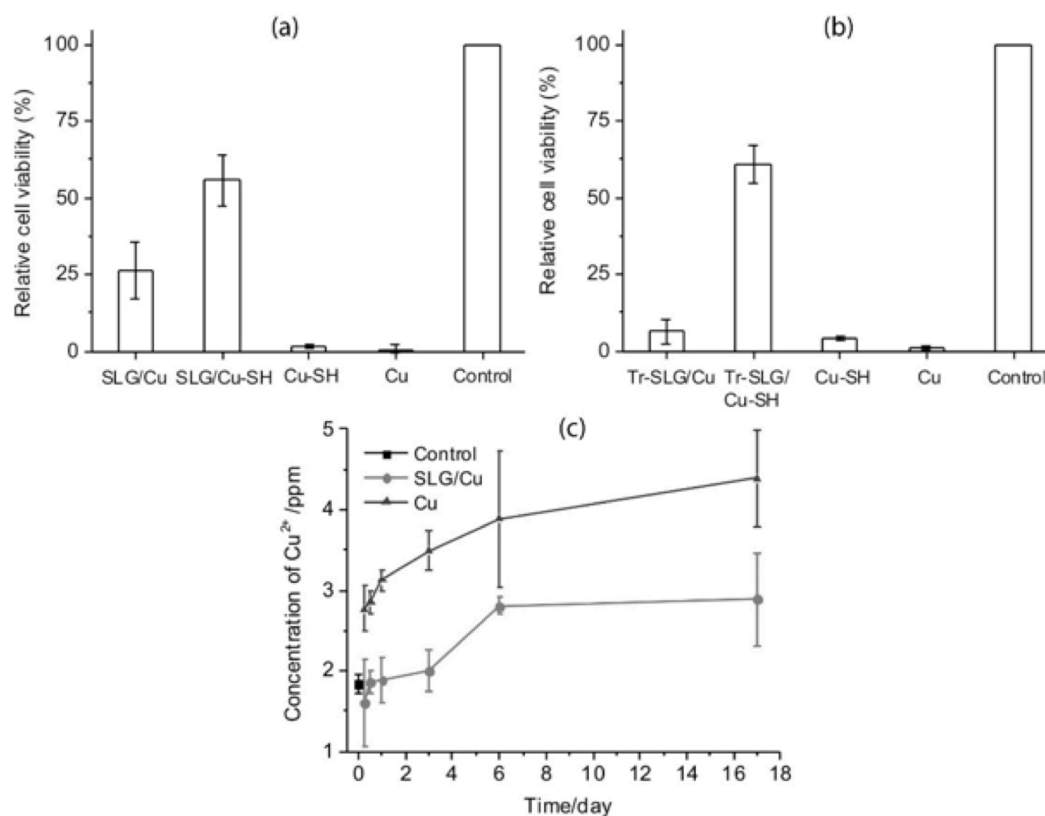
Figure 10: Relative cell viability of (a) bone cells incubated with SL Gr and SL Gr/Cu-SH, Cu-SH and bare Cu foil for 3 days. Control is a regular cell culture without Cu foils; (b) Relative cell viability of bone cells incubated with Tr-SL Gr/Cu, bare Cu, Tr-SL Gr/Cu-SH, and Cu-SH for 1 day; (c) Concentrations of Cu(II) ions in blood samples extracted from live rats with concentrations of Cu(II) from normal rats before implantation as control (black square), rats with implanted SLG/Cu foils (blue triangles) and rats with implanted Cu foils (red dots) as a function of time [79] (republished by courtesy of the publisher, Nature Publishing Group)

suitable to work out and implement practical deposition methods for atom-thick films on various metals, although a different approach must be applied for Newtonian [101] and non-Newtonian fluids [102]. Uniform coatings can be obtained over large areas with reproducible thicknesses in a good controllable manner, but only on planar substrates, which is a major limitation of this technique. SC starts by applying a small puddle onto the centre of the substrate, then spinning commences at initially a lower then, within a matter of seconds, at a higher rotational speed (two stages of centrifugation up to ~3000 rpm). The centrifugal force and centripetal acceleration result in excessive spreading of the fluids on the surface (wetting and covering depend on multiple physical-chemical parameters) and an inevitable loss (can be recycled) around the edges of the substrate until the spin-off time is completed. Then, a thin film forms releasing solvents and curing takes place, because of chemical reactions.

Kinetic Spray

Kinetic spray (KS) utilises a Laval nozzle to spray Gr colloid solutions at a very high speed and the supersonic acceleration leads to the production of very small droplets that evenly disperse then evaporate reducing the tendency of flake aggregation. Besides the uniform and smooth layers, defects in the Gr flakes were not observed. Hence, high quality film production by KS depends on the energy of the impact stretches Gr sheets then carbon atoms arrange into flawless hexagons based on plasticity probing of the Gr flakes [103]. Transmittance of graphene oxide (GrO) film spray deposited on soda-lime glass (from a 10 wt.% colloid solution of GrO in ethanol) was 73% and sheet resistance was 19 kΩ sq^{-1} using incident light at the wavelength of 550 nm. The electrical conductivity of the coatings increased by up to a thousand times after hydrazine reduction and annealing at 400 ºC. Additional thermal annealing at 1100 ºC further enhanced conductivity by ca. 10 times. Soda-lime glass with a transparency of 80% and electrical conductivity of 209 S cm^{-1} (or sheet resistance; R_s = 2 KX sq^{-1}) as applied to a 14 nm thick Gr film [104]. KS is a reliable technique of wide commercial availability and offers a flexible solution to large-scale using according to recently reported corrosion tests [105-107].

Electrospinning

Electrospinning (ES) creates polymer fibres with a diameter range of between 40 and 2000 nm. The fibres can be made from solutions or from fused materials, controlling diameter size through the adjustment of

surface tension, solution concentration, conductivity and so forth [108-110]. ES occurs when the electric force of the surface overcomes the surface tension of the fluid phase triggering an electric spark, results in the solution being expelled from a syringe forming jet flow impacts and deposits. When the expelled material dries out or solidifies, it forms an electrically charged fibre that can be directed or speeded up by electric forces. So, a polymer solution stored in a syringe is charged to a high electrical potential. As the jet stretches and dries, radial electrical forces cause it to splash repeatedly. Dried, solidified fibres are collected on an electrically conductive (metal) screen. By ES, the composition of nylon 6-6 and Gr was prepared and deposited on porous silica then tested under various conditions [111]. Oxidation and reduction potentials in acidic, alkaline, and peroxide solutions were assessed by dynamic polarisation. SEM observations determined that treatment with acidic and basic solutions led to the formation of solid aggregates and slightly folded GrO flakes. Thermal treatment at 700 ºC gave samples with a porous structure. After annealing, a subsequent chemical derivatisation with acidic, basic and peroxide solutions assisted with ultrasonication facilitated the separation of GrO sheets, leading to a solid composed of lower dimensional flakes, especially in the case of oxidation. Oxidation was carried out in KOH and the reduction in H_2SO_4 solution. EIS data obtained in the immersion test with a Na_2SO_4 solution indicated decreasing interfacial capacitance of the ES produced samples with the Ny-GrO coatings. The EIS data calculated at 0.8 Hz changed between $1.4–4.5×10^{-5}$ and $7.5–8.9×10^{-7}$ F cm^{-2} (depending on the concentration of the electrolyte) with the GrO content increasing from 0.4 wt.% to 2 wt.%.

Electrophoresis

Electrophoretic deposition (EPD) is a promising technique to fabricate functionally graded [112-114] and hybrid composites [115, 116], laminated nano-ceramics [117, 118], and functional, nanostructured films and coatings [119-121]. In the last couple of years, numerous EPD applications have emerged as industries count on commercial advantages over other fabrication routes. It is a versatile and cost effective technique with acceptable levels of control over microstructure, stoichiometry, and macroscopic-microscopic dimensions and properties [122, 123]. EPD is a two-step colloid process in which electrostatically charged particles, suspended in a liquid medium, migrate according to the electric field towards the oppositely charged electrode. Then particles deposit, and flocculate on the electrode surface forming a relatively dense, homogeneously packed, bonded layer. Increasing the volume fraction of the nanoparticles and their deposition on the surface of any electrically conductive material is relatively easy. Usually, a post-treatment is required to increase the density of deposits and eliminate porosity [122]. Sometimes special modifications are required to render surfaces with

notable properties such as increasing hydrophobicity by silylation. EPD is performed in stable colloid solutions in which there are plenty of electrostatically charged particles migrating in response to an impressed DC electric field and deposit either as a loose homogeneous or compact film onto the oppositely charged electrodes. To make deposits denser and eliminate porosity, additional EPD or heat treatment is required. Oxide particles, conductive polymers [124] and highly dispersed activated carbon [125] of nearly any size in colloidal suspensions [122] were deposited by this method, reflecting its high versatility. Furthermore, by electrophoresis uniform thin layers can be made on highly ragged, complex surfaces. Moderate electrical conductivity of the resulting substrates is the only requirement. The sample surface is treated as a whole in a uniform manner, whereas dimensions, deposition rate, uniformity and scale up features are also favourable. EPD is a preferable alternative to many other methods like slurry dipping, thermal and plasma spraying, sputtering, and physical/chemical vapour deposition.

In the course of thick Gr layer deposition on copper by EPD [126], deoxygenation of carbon was hinted at by bathochromic shifts in the UV spectra because of the electrochemical configuration and reaction mechanism. Potentiodynamic scanning showed positively shifted corrosion potentials and lower corrosion currents (I_{corr}), which suggested only mediocre protection by the thick Gr films in the initial phase of immersion propagation.

The composite coating of reduced GrO was prepared by cathodic EPD in an aqueous solution in a symmetrical cell-electrode arrangement [127]. Optimum conditions for cathodic deposition were found to produce a thickness of ~40 nm by applying 10 V for 30 s. SEM observations revealed the size of the GrO sheets being 1–2 µm, covering the surface uniformly. The composite coating was shown to protect copper firmly from electrochemical corrosion. Potentiodynamic measurements indicated an ennobled free corrosion potential with slightly reduced anodic and cathodic current branches, suggesting a lower corrosion rate of the composite coated copper compared to its bare form during the early phase of propagation. Experimental conditions are summarised in *Table 2*.

By electrophoresis, GrO was uniformly deposited on a permanent magnet, e.g., NdFeB and the coating was subsequently reduced to partially remove functional groups containing oxygen [128]. The EPD GrO coating showed substantially better adhesion to the substrate compared to the spin-coated ones. The surface of the bare NdFeB was rough and porous but site-dependent topography of the EPD-GrO modified samples depended on the amount loaded. The relationship between the increasing thickness and decreasing adhesion of the coating with an extension of deposition time was determined. Raman, infrared, and X-ray photoelectron spectroscopy (XPS) results reflected the strong adhesion of EPD films and that was connected to the Koble-type decarboxylation mechanism [129, 130] of the surface yielding GrO flakes. An unexpected outcome was that several deterioration reactions were observed in GrO. The signal of epoxy groups decreased

Table 2: Metallic substrate, type and growth parameters to obtain Gr film by EPD and chronoamperometry

Substrate	Preparation types and their parameters	Corrosion test parameters	Work-electrode surface (cm^2)	Types of potentiodynamic tests	Ref.
Cu	GrO, EPD in sol. C = 1.0 mg cm^{-3}, E=1 V / 10 mm^{-1}, 10 min	air ox. at 200 ºC for 4 h, in 30 wt.% H_2O_2 for 2 min, then 0.1 M NaCl solution	Unknown	after 1 h at OCP, scan rate: 1 mV s^{-1}	[131]
Cu	red. GrO with polyiso-cyanate cured with HAA (hydroxyl acrylic acid), EPD for 30 s, at E = 10 V 10 mm^{-1}, 0.1 M $NaBH_4$ red. for 5 min	3.5 wt.% NaCl, at 25 ºC	1	after 2 h at OCP, scan rate: 1 mV s^{-1}	[132]
NdFeB	GrO red., EPD in sol. of 1 mg cm^{-3} GrO, NdFeB anode & Pt cathodic dep., E=10 V / 10 mm^{-1},	3.5 wt.% NaCl solution at room temperature	Unknown	EIS	[133]
Cu	GrO isocyanate cured with hydroxy acrylic, then silylation, EPD on Cu at 10-30 V 10 mm^{-1}	3.5 wt.% NaCl, at 25 ºC	1	EIS	[136]
Cu	chronoamperometry of GrO at −1.5 V for 10 min in sol. C = 2 g dm^{-3}, in 0.1 M KCl, at −1.5 V for 10 min, then GrO red. $NaBH_4$ (0.1M) for 5 min	OCP 3.5 wt.% NaCl sol. after 1 h	1	EIS	[138]
Mild steel	EPD in Ni sol. at pH = 3, Iρ = 1 A dm^{-2}, at t = 40ºC, Gr c=100 mg dm^{-3}	3.5 wt.% NaCl, at 27 ºC	1	scan rate: 0.01 V s^{-1}, EIS	[169]

after deposition, which might be explained by the high anodic electrode potential applied to the working electrode and the large potential drop at the interface. The decrease in current density during potentiodynamic scanning and the positive shift in the free corrosion potential of the system reflected efficient initial protection but lower cohesion and adhesion of the thicker coatings, leading to a poorer protection potential.

The GrO-acrylic polymer composite fully covered the copper substrates, but the sheets were separated far from one another in an island like manner consequently a large percentage of the surface remained unburied [131]. As for the reagents, solution and cell arrangement, EPD conditions e.g. voltage (10 V) and deposition time (30 s) proved to be optimal to obtain crack-free films of an average thickness of 45 nm. An electrochemical investigation indicated insignificant protection performance of the composite coating under immersion propagation. A steady corrosion current extrapolated to the OCP region showed slight changes over the anodic and cathodic regions. A current density drop of 38.3–3.5 μA cm^{-2} was observed in comparison to the bare copper. A polarisation resistance of the composite covered specimen was assessed by EIS, assigning an increased charge-transfer resistance of ~25 Ω cm^{-2} (bare copper: ~8 Ω cm^{-2}).

Stainless steel specimens with an exposed geometrical surface of 100 cm^2 were almost uniformly deposited with GrO in H_2SO_4 solution by coupling the substrate cathodically [132]. For transferring purposes, chemical and electrochemical etching was developed to delaminate the reduced GrO film, giving coherent freestanding membranes or deposit them onto other substrates. By optimising electrophoretic parameters, a low voltage of 3 V was found to consolidate reduced GrO layers preferentially aligned in an in-plane direction through a cohesive electrophoretic squeezing force in near volume range of the electrode (cathode). The free-standing Gr membrane was reduced, annealed at 1000 ºC then a graphite-like architecture evolved with a d-spacing of 3.42 Å and C/O ratio of 16.7. Electrical conductivity was of high as 5.5×10^5 S m^{-1}.

Graphene Coated Metals in Electrochemical Cells and Batteries

Because corrosion is a serious problem in energy storage devices like batteries and fuel-cells [133], the application of GrO as a barrier coating to inhibit the corrosion of aluminium electrodes in lithium ion batteries is considered to be an innovative solution. Spin-coating was employed to coat aluminium with GrO and decrease the corrosion rate when the electrode was subjected to the electrolyte of $LiPF_6$ (1.0 M) dissolved in ethylene carbonate and dimethylcarbonate (50:50 vol.%) [134]. SEM observations with energy dispersive X-ray spectroscopy analysis and atomic force microscopy (AFM) scanning suggested increasing surface roughness of aluminium with lower GrO quantity, but its greater amount helped reduce the roughness remarkably. The average roughness of the bare substrate was around 350 nm, which changed to 199-154 nm for the GrO loaded one. The thickness of the film showed great epitaxial variety even though the coating was relatively thick. Cyclic voltammetry showed a decreasing electrochemical current response of the GrO coated electrodes with increasing surface loading. This indicated hindered and impeded charge-transfer through the electrode interface without any direct implication of capacitive and adsorption charge loss in the current transients. Accordingly, chrono-amperometry curves exhibited moderately changing characteristics (as a consequence of altered electrode kinetics) in the early phase of the transients and

decreasing base currents over the complete timescale because of the smaller electroactive surface. EIS spectra suggested a somewhat higher resistance against pitting, the lower susceptibility to localised corrosion. Thus, GrO restricted aluminium oxidation, behaving as a charge-transfer barrier. Otherwise, the lower capacity and potential of the cells should have been measured by the set-ups with the GrO loaded electrodes during charge–discharge testing. Instead, surprisingly the opposite was reported. Nevertheless, enhanced cycle-life stability (lower rate of capacity loss) of the modified electrode compared to the cell configuration with bare aluminium is of course self-explanatory. Self-discharge was lower as a decreasing rate of open circuit voltage decline was observed to the modified aluminium samples. GrO films did not show any corrosion and the underlying native oxide layer remained intact under test conditions.

Microbiologically induced corrosion (MIC) severely limits the structural integrity and lifetime of metallic structures in technological processes and applications because of frequently evolving mechanisms, i.e., crevice and pitting local corrosion phenomena. A microbial fuel cell (MFC) is a galvanic cell producing an electric current that causes bioelectro-chemical oxidation of organic substances on anodes and abiotic reduction on cathodes [135]. MFCs have been used as a galvanic tool to simulate extracellular electron transfer mechanisms of microbes and the bio-electrochemical oxidation of organic substances. In addition, metals are not used as anodes in MFCs due to their fast galvanic corrosion. Owing to this, Gr films are employed as barrier coatings and the corrosion rate of the working nickel electrode was evaluated by galvanic coupling in the MFC set-up [136]. Regarding the experiment, it was determined that the geometrical ratio of the working and counter electrodes was the guarantee to maximise, and concentrate current densities on the working electrode.

Nevertheless, the cell design did not allow the assessment of adequate kinetic parameters (general corrosion rate) because of the large uncompensated ohmic drop and unfavourable cell geometry. These are all relevant in DC techniques, although inadequate voltammetric data could provide a rough estimation, even though 5 mV s^{-1} was higher than recommended and might have resulted in the considerable rate of adsorption and pseudo-capacitive current during the measurement. In relation to the impedance measurement and its evaluation, these data are even more sensitive to inappropriate cell design. The protection efficacy of the Gr film was assessed under realistic operating conditions, the bare and coated nickel electrodes represented a 3D microporous structure. The overall outcome confirmed a retardation of corrosion processes by the Gr film for extended periods. CV scanning showed decreased current transients of coated nickel, which was ca. ten thousand times lower than measured for the bare nickel electrode based MFC after a propagation for 2800 h. Nickel dissolution rates of the Gr coated anodes were at least ten times lower than the baseline (uncoated) electrode. EIS characterisation confirmed impeded MIC on the Gr/nickel for ca. 40

folds in comparison with uncoated electrodes. The effective masking of nickel from the mixture of microorganisms and their metabolic products was concluded.

Composite Graphene Coatings

Physically Mixed and in situ Polymerised Mixtures

Chronoamperometry was successfully employed to prepare Gr coated copper, starting from an aqueous colloid solution of GrO [137]. As a result of the EPD process, a seemingly compact and void of area without coating; and polymer film with Gr inclusion was obtained. Nevertheless, the distribution of Gr flakes was highly uneven and inhomogeneous (random), whereas the sheets showed various degrees of folding and overlapping in the polymer matrix. In addition, the fast reduction of GrO in the polymer proves the high permeability of the matrix, although it reached a thickness of several micrometres. On the other hand, the coatings with reduced GrO provided moderate protection for copper with an initial inhibition rate of 94% drawn from the potentiodynamic polarisation measurement data (at nil impressed potential). The corrosion rate reduced to 0.2 mm yr^{-1} from the rate for pure copper of ca. 3.65 mm yr^{-1}. This assessment was only made at the beginning of the immersion test (after an hour), whilst waiting for stabilisation of the freshly installed cell set-up. In comparison with the EIS investigation, the composite coating provided electrical insulation and ionic diffusion hindrance to the copper surface. So, the protection was related to the increased polarisation resistance of Gr loaded coatings of ca. 26 Ω cm^2 compared to bare copper of 9 Ω cm^2.

Intrinsically conducting polymers (ICPs) like electroactive polyaniline (PAni) have been widely used materials for some time providing corrosion protection regardless of the long-standing disagreement over the anodic protection mechanism and the generally less effective barrier nature. PAni is a preferable electron-conducting polymer with favourable properties over other alternatives. Under optimal conditions, the protection mechanism leads to the formation of a passive (dense) metal oxide layer [138-140].

To increase protection performance, many substances such as well dispersed clay [141] with an aspect ratio of ca. 200 was aimed at lengthening mass transport pathways through the composite films for all redox active species. These polymer-clay mixtures exhibited notable protection improvements over neat polymers. Besides the several attempts to combine of carbon nanotubes (CNTs) with organic [142-156], inorganic, and metal [157-160] matrixes for corrosion protection and resistance, respectively, there are examples from the literature about testing Gr-polymer composites for various purposes [160-162]. The main focus of these works was the exploitation of high relative aspect ratio of Gr (ca. 500) [163] in comparison to exfoliated clay minerals. Hence, Gr is a key filler in advanced gas barrier materials, motivating studies to

Table 3: Metallic substrate, type and growth parameters to obtain Gr films by spin coating and solution casting. Types and settings of corrosion tests and electrodes with the reference number of the article

Substrate	Preparation type and parameters	Corrosion test parameters	Work-electrode surface (cm²)	Types of electrochemical tests	Ref.
porous silica	electrospin Gr-Nylon 6-6 in formic acid agitated for 12 h then add. of GrO, ES at 12 kV, flow rate: 0.2 mL h⁻¹ for hours, Electrode: polymer solution 90 wt.% of formic acid with 0.36-2 wt.% GrO and Ny	Potentiostatic oxidation in KOH (0.5 M) for 3.5 h, reduction in H_2SO_4 at pH = 2 for 8 h, EIS in Na_2SO_4 in (1-10^{-1}-10^{-2}-10^{-3} M) for hours	unknown	potentiostatic treatment, potentiodynamic polarisation, scan rate: 100 mV min⁻¹, EIS	[112]
AlO$_x$	GrO sonication in ethanol then spin-coating	LiPF$_6$ in ethylene carbonate and dimethyl-carbonate (50:50 vol.%); at 1.0 M	100	cyclic voltammetry, chronoamperometry, potentiodynamic polarisation and EIS	[114]
Cu	Spin-coating of Gr with acetone (20 cm³ cm⁻²) then rapid annealing 800-1000 ºC for 3 min	Seawater 3.0–3.5% NaCl	0.25	potentiodynamic polarisation, scan rate: 2 mV s⁻¹, EIS	[136]
steel	PAni-Gr comp. (NMP complex and casting)	3.5 wt.% NaCl solution	unknown	potentiodynamic polarisation	[153]
cold-rolled steel	GrO red. with N_2H_2, pressing powders then curing (thickness: ~120 μm)	3.5 wt.% NaCl, at 25ºC	1	potentiodynamic scanning at 10 mV min⁻¹, after 30 min EIS	[161]
low alloy steel	2 wt.% Gr/MWCNT/PEI & 20 wt.% Gr/PEI comp.-s, dispersion in PAA cured at 150 ºC for 5 min, then 250 ºC for 5 min for imidisation	3.5 wt.% NaCl solution	9.62	potentiodynamic polarisation (scan rate: 1.67 mV s⁻¹)	[7]
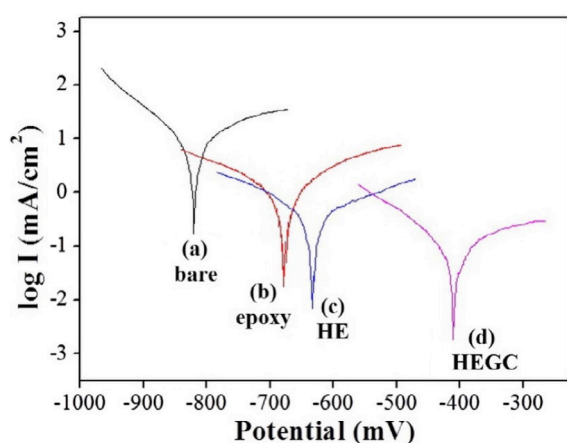
Figure 11: Tafel plots of the (a) bare, (b) epoxy-coated, (c) HE coated, and (d) HEGC-coated CRS electrodes [178] (by courtesy of the publisher, Elsevier)

achieve very low oxygen permeability using low filler contents (compared to neat polystyrene and the best polymer-clay mixture known at that time) [164] and underscore the possible obliteration of traditional clay-polymer composites [165-169]. Thus, a carefully designed and well-prepared PAni-Gr mixture exhibited outstanding impermeability characteristics against the diffusion of molecular oxygen and water vapour *versus* neat PAni and PAni-montmorillonite using a filler content of 0.5 wt.% and the excellent protection performance of steel substrates. Potential ennoblement of steel electrodes with coatings of increasing Gr content was considerable and an approximately fifteen times lower steady corrosion current was reported. The main reason for the success is mostly related to the high dispersity of Gr in the composite of microscopically isolated and macroscopically non-percolating

distribution [170]. Experimental conditions are summarised in *Table 3*.

Lower electrical and ionic conductivities always provide better corrosion protection. Therefore, metals coated with Gr filled composites of electrically less or non-conducting (practically insulating) matrices like epoxy (in the case of high dispersity) can behave as a super-hydrophobic interface [171-176]. These composites are characterised by a water contact angle of at least 150º making them repellent, resistant to water absorption [177] and their exceptionally good anti-wetting properties results in good corrosion prevention potentials.

The nano-casting prepared epoxy-Gr composite featured high hydrophobicity and provided excellent protection for cold-rolled steel (CRS) panels [178]. *Fig.11* shows Tafel plots of bare, epoxy, hydrophobic epoxy (HE) and hydrophobic epoxy-Gr composite (HEGC) coated CRS panels. The open circuit potential of the immersion tested steel panels coated with epoxy-Gr showed appreciable ennoblement of ca. 0.3 V and ca. ten times lower corrosion currents compared to neat epoxy coated steel. The much higher polarisation resistance was partly attributed to the more hindered mass transport through the Gr loaded coating (with less than half the oxygen permeability) and access to its interface on the fluid side as a result of the finely patterned structure of the outer surface. The reproducibility of the data is questionable because parameters were not representative to properly describe the kinetic processes of the system, proceeding at the metal-solution interface. As in other cases, electrochemical techniques gave instantaneous rate assessments (in the first 30 min of the tests). Thus, the reported data are not suitable for forecasting long-term corrosion rates.
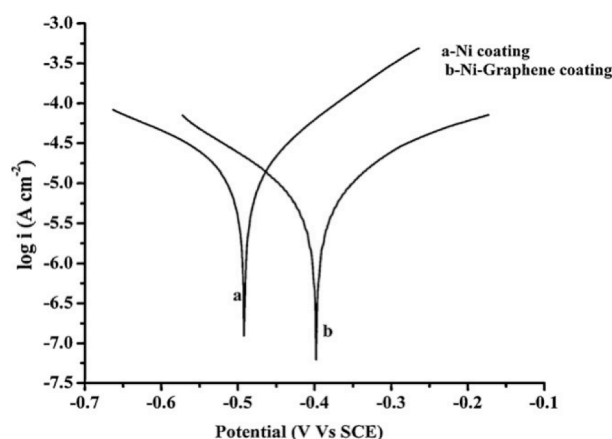
Figure 12: Tafel curves of Ni and Ni–Gr materials [186] (by courtesy of the publisher, Elsevier)

Figure 13: Cryo-fractured SEM images of (a) and (b), PEI, (c) and (d) 2 wt.% NFG/MWCNT/PEI, (e) and (f) 20 wt.% UNFG/PEI [187] (published with permission from the American Ceramic Society Bulletin)

A more exotic approach is to develop metal-Gr composites for corrosion protection, although this strategy may have more disadvantages than advantages like with the metal-CNTs [179-182] because of the CNT activity towards catalytic oxygen reduction reactions [183-185]. Electrodeposited thin films of nickel matrix with Gr inclusion indicated a slight improvement in general protection performance; ennobled OCPs by ~0.1 V and steady corrosion currents reduced by over 50% were observed in comparison with pure nickel coated mild steel [186]. As a result of greatly affected nucleation and growth rate, measurement results are much more related to the highly altered crystalline structure of the nickel host matrix (lower electrical conductivity was unfortunately not characterised) as a consequence of the inclusion of Gr sheets, but differences in the texture and hardness of pure nickel and the Gr-nickel coatings were reported. Similarly to many other works, protection efficacy was not evaluated and reported over long-term immersion testing. On the one hand, the Tafel analysis of Ni and Ni–Gr performed in 3.5 wt.% NaCl solution (in *Fig.12*) was carried out using high voltage rate scanning without ohmic drop compensation, leading to distorted current legs over both potential regions (from the open-circuit or free corrosion potential of the electrode). A less representative transient is due to the low proportion of Faradaic charge-transfer current primarily assigned to the credible corrosion rate assessment. Probably due to these reasons, there is not much difference between the given corrosion currents of Ni and Ni-Gr samples. The Gr incorporation, cathodic and anodic Tafel regions exhibited almost ideal symmetry. This should mean the same scale of activation (expressed as a transfer function) in the cathodic (reduction and deposition) and anodic (oxidation and dissolution and/or deposition) processes. This feature is a kind of ineffectively blocked electrode behaviour, a quite reversible characteristic with less viable hindrance either in the anodic or cathodic processes. This suggestion seems to be confirmed by the reported similar corrosion currents.

On the other hand, the adequacy of EIS data may also be doubtful as basic requirements of system stability (in the time domain), linearity (immediate response), and causality (the unquestionable relationship between perturbation and type-degree of response) might not be met. The time frame of 5 min to wait for a stationary or a steady-state condition then making measurements is in itself questionable. The large variation in the solution resistance (between the pure and composite Ni coating) is surely inadequate. In addition, the highly varied interfacial and coating resistance (swop between them) along with a hundred times difference in the coating capacitance are also unbelievable and can lead only to false interpretation. The depressed semicircle is a result of the complexity of the Ni/Gr electrode interface. The electrode was a porous electron and ion conductor and such systems need to be carefully handled (modelled with at least two transmission lines) when evaluation of impedance spectra in relation to structure and mechanistic behaviour of a complicated interface comes into the picture. Therefore, presented data and the corresponding evaluation are not appropriate and even misleading.
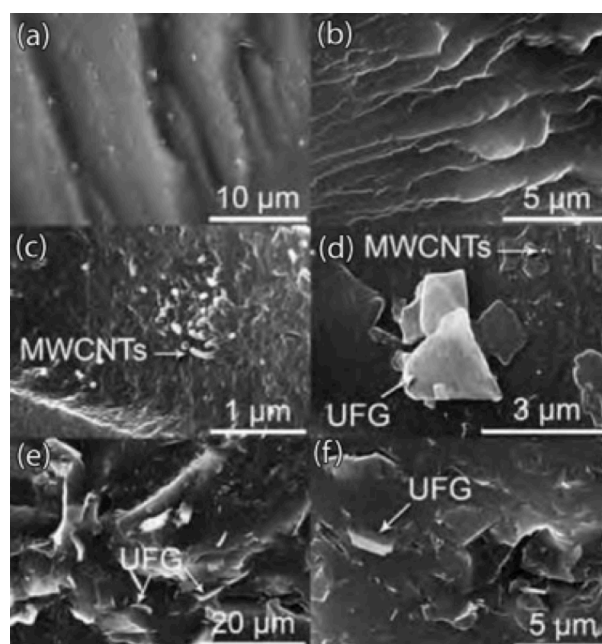
An innovative approach is the composite of multi-walled CNTs (MWCNTs) and exfoliated Gr embedded in polyether-imide (PEI) serving as a coherent and pore-free matrix [187]. This endeavour was made in an attempt to achieve a uniform dispersion of the nano-size additives in the host matrix (without functionalisation of the filler phase) and good adhesion of tailored PEI to the substrate, facilitating the maximum attainable corrosion protection performance. The protection mechanism was delineated according to the following: the composite protects steel alloys by a complex, active–passive way, serving as a physical barrier to water permeation against the evolution of ion channels to the metal surface and passivating metal surface by electron depletion at the interface based on the Schottky barrier effect [188-190].

Exfoliated but non-functionalised Gr was derived from ultrasonication in a solution of N-methyl-pyrrolidone (NMP). PEI as a host matrix was selected for its flexibility under a high glass transition temperature (155 ºC), thermal stability, firm resistance against radiation and appropriate interaction with carbon fillers *via* π–π stacking [191-193]. *In situ* synthesis and the imidisation protocol yielded coatings with appropriate adhesion properties to the steel surface of a thickness of 15–20 μm, whereas agglomeration and phase segregation of the fillers were low with the MWCNTs.

The SEM investigation revealed a fairly smooth surface finish without cracks or visible pinholes in the coatings. No phase segregation of the Gr and MWCNT fillers was observed in the mixtures around the interface as its clearly seen in *Fig.13* of the cryo-fractured samples of non-functionalised Gr (NFG), carbon nanotubes and PEI in 2 wt.% (c and d) and NFG/PEI of 20 wt.% (e, f) in comparison with pure PEI (a and b). OCPs were positively shifted by ~0.6 V, meaning a remarkable ennoblement. This was inferred, although substrates with high resistance coatings showing notable positive potentials must be at least partially attributed to the potential drop through the coatings [194] as a result of masking the real corrosion potential of the metal-coating interface to various extents. A potentiodynamic test indicated current densities of several orders of magnitudes lower ($\sim 10^{-9}$ A cm^{-2}) for composite coated specimens compared to bare low-alloy and galvanised steel samples with current densities of $\sim 10^{-5}$ A cm^{-2}. Immersion tested samples were characterised quantitatively with regards to the perspective of corrosion rate or protection of steel substrates by weight-loss measurement (according to the ASTM-G1 protocol) after 3,144 hours. The substrate coated with 20 wt% Gr-PEI performed best with ca. thousand times lower corrosion rates (ca. 8.5×10^{-4} mm year^{-1}) than bare low-alloy steel samples (ca. 1.2×10^{-1} mm year^{-1}). However, the PEI film containing Gr and MWCNT (ca. 9.2×10^{-3} mm year^{-1}) manifested a moderate average corrosion rate of ca. 5.5×10^{-4} mm year^{-1} compared to the neat PEI film.

Concluding Remarks

Overall, it is evident that atomic pure graphene films lack uniformity and partly this leads to insufficient instantaneous protection performance. Therefore, some sort of physical and/or chemical post-treatment is needed to facilitate long-term protection performance

From direct deposition techniques, the broadly and thoroughly investigated CVD technique is undoubtedly a viable alternative when large-scale continuous surface finishing is highly demanded. However, it is far from the best choice when corrosion protection efficiency and durability are the priorities, due to the complexity of growing cohesive films on the surface of metal substrates with preferable orientation of the grains, and weak adherence of Gr films sensitive to mechanical and surface charging effects.

When performance is an essential preference then spin-coating, kinetic spray, electro-spinning, and electrophoretic deposition should be employed depending on the complexity of the surface, conductivity of the substrate and additional technological aspects in relation to further processes. Among them, spin-coating and kinetic spray techniques develop good quality and homogeneous coatings of greatly varied thicknesses. Thin and ultra-thin films feature high a dispersity, and an even distribution and sometimes even improved quality of the nanoparticles. When thicker coatings are obtained on electrically conducting substrates with strong adhesion to complex surface geometries without the matter of a certain degree of alteration of the nanoparticles, then electrophoretic deposition must be used.

With respect to the utilisation of pure ultra-thin Gr films and thicker coatings as Gr-filled composites, there are ways to achieve further progress in relation to the ultimate aim of improved corrosion protection. For example, thin Gr films can still be used as a primary metal surface finishing. Alternatively, strongly adhering matrices with Gr filler might obviously mean a far more robust solution with protection efficacy targeting high performance demands for real situations. Parameters like the combination and concentration of the fillers, and compatibility with the host matrices besides matching complementary technological requirements need to be carefully optimised to gain appropriate barrier and/or inhibition functions.

REFERENCES

[1] NOVOSELOV K.S., GEIM A.K., MOROZOV S.V., JIANG D., ZHANG Y., DUBONOS S.V., GRIGORIEVA I.V., FIRSOV A.A.: Electric Field Effect in Atomically Thin Carbon Films, Science, *2004*, 306(5696), 666–669

[2] NOVOSELOV K.S., GEIM A.K., MOROZOV S.V., JIANG D., KATSNELSON M.I., GRIGORIEVA I.V., DUBONOS S.V., FIRSOV A.A.: Two-dimensional gas of massless Dirac fermions in graphene, Nature, *2005*, 438(7065), 197–200

[3] BALANDIN A.A.: Thermal properties of graphene and nanostructured carbon materials. Nat. Mater., *2011*, 10(8), 569–581

[4] RAFIEE J., MI X., GULLAPALLI H., THOMAS A.V., YAVARI F., SHI Y., AJAYAN P.M., KORATKAR N.A.: Wetting transparency of graphene, Nat. Mater., *2012*, 11(3), 217–222

[5] RAFIEE J., RAFIEE M.A., YU Z.-Z., KORATKAR N.: Superhydrophobic to superhydrophilic wetting control in graphene films, Adv. Mater., *2010*, 22(19), 2151– 2154

[6] SUTTER P., MINNITI M., ALBRECHT P., FARÍAS D., MIRANDA R., SUTTER E.: A high-reflectivity, ambient-stable graphene mirror for neutral atomic and molecular beams, Appl. Phys. Lett., *2011*, 99(21), Art. No. 211907

[7] BUNCH J.S., VERBRIDGE S.S., ALDEN J.S., VAN DER ZANDE A.M, PARPIA J.M., CRAIGHEAD H.G., MCEUEN P.L.: Impermeable atomic membranes from graphene sheets, *2008*, Nano Lett., 8(8), 2458–2462

[8] NAIR R.R., WU H.A., JAYARAM P.N., GRIGORIEVA I.V., GEIM A.K.: Unimpeded permeation of water through helium-leak-tight graphene-based membranes, Science, *2012*, 335(6067), 442–444

[9] LEENAERTS O., PARTOENS B., PEETERS F.M.: Graphene: a perfect nanoballoon, Appl. Phys. Lett., *2008*, 93(19), Art. No. 193107

[10] BERRY V.: Impermeability of graphene and its applications, Carbon, *2013*, 62(1), 1–10

[11] CHEN S., BROWN L., LEVENDORF M., CAI W., JU S.-Y., EDGEWORTH J., LI X., MAGNUSON C.W., VELAMAKANNI A., PINER R.D., KANG J., PARK J., RUOFF R.S.: Oxidation resistance of graphene-coated Cu and Cu/Ni alloy, ACS Nano, *2011*, 5(2), 1321–1327

[12] LIU L., RYU S.M., TOMASIK M.R., STOLYAROVA E., JUNG N., HYBERTSEN M.S., STEIGERWALD M.L., BRUS L.E., FLYNN G.W.: Graphene oxidation: thickness-dependent etching and strong chemical doping, Nano Lett., *2008*, 8(7) 1965–1970

[13] SURWADE S.P., LI Z.T., LIU H.T.: Thermal oxidation and unwrinkling of chemical vapor deposition-grown graphene, J. Phys. Chem. C, *2012*, 116(38) 20600–20606

[14] PRASAI, D. TUBERQUIA J.C., HARL R.R., JENNINGS G.K., ROGERS B.R., BOLOTIN K.I.: Graphene: corrosion-inhibiting coating, ACS Nano, *2012*, 6(2), 1102–1108

[15] DE HEER W.A., BERGER C., WU X., FIRST P.N., CONRAD E.H., LI X., LI T., SPRINKLE M., HASS J., SADOWSKI M.L., POTEMSKI M., MARTINEZ G.: Epitaxial graphene, Solid State Comm., *2007*, 143(1-2) 92–100

[16] SHIVARAMAN S., CHANDRASHEKHAR M.V.S., BOECKL J., SPENCER M.G.: Thickness estimation of epitaxial graphene on SiC using attenuation of substrate Raman intensity, J. Electron. Mater., *2009*, 38(6), 725–730

[17] RATINAC K.R., YANG W., GOODING J.J., THORDARSON P., BRAET F.: Graphene and related materials in electrochemical sensing, Electroanalysis, 2011, 23(8)3, 803–826

[18] BROWNSON D.A.C., MUNRO L.J., KAMPOURIS D.K., BANKS C.E.: Electrochemistry of graphene: not such a beneficial electrode material? RSC Adv., *2011*, 1(6), 978–988

[19] RAMAN R.K.S., TIWARI A.: Graphene: The thinnest known coating for corrosion protection, J. Org. Materials, *2014*, 66(4), 637–642

[20] TONG Y., BOHM S., SONG M.: Graphene based materials and their composites as coatings, Austin J. Nanomed. Nanotechnol., *2013*, 1(1), 1–16

[21] REINA A., JIA X., HO J., NEZICH D., SON H., BULOVIC V., DRESSELHAUS M.S., KONG J.: Large area, few-layer graphene films on arbitrary substrates by chemical vapor deposition, Nano Lett., *2009*, 9(1) 30–35

[22] KIM K.S., ZHAO Y., JANG H., LEE S.Y., KIM J.M., KIM K.S., AHN J.-H., KIM P., CHOI J.-Y., HONG B.H.: Large-scale pattern growth of graphene films for stretchable transparent electrodes, Nature, *2009*, 457(7230), 706–710

[23] CORAUX J., N'DIAYE A.T., BUSSE C., MICHELY T.: Structural coherency of graphene on Ir(111), Nano Lett., 2008, 8(2), 565–570

[24] SUTTER P.W., FLEGE J.-I., SUTTER E.A.: Epitaxial graphene on ruthenium, Nat. Mater., *2008*, 7(5), 406–410

[25] LI X., CAI W., AN., KIM S., NAH J., YANG D., PINER R., VELAMAKANNI A., JUNG I., TUTUC E., BANERJEE S.K., COLOMBO L., RUOFF R.S.: Large-area synthesis of high-quality and uniform graphene films on copper foils, Science, *2009*, 324(5932) 1312–1314

[26] LEE Y., BAE S., JANG H., JANG S., ZHU S.E., SIM S.H., SONG Y.I., HONG B.H., AHN J.H.: Wafer-scale synthesis and transfer of graphene films, Nano Lett., *2010*, 10(2), 490–493

[27] LI X.S., ZHU Y.W., CAI W.W., BORYSIAK M., HAN B., CHEN D., PINER R.D., COLOMBO L., RUOFF R.S.: Transfer of large-area graphene films for high-performance transparent conductive electrodes, Nano Lett., *2009*, 9(12), 4359–4363

[28] PARK H.J., MEYER J., ROTH S., SKÁKALOVA V.: Growth and properties of few-layer graphene prepared by chemical vapor deposition, Carbon, *2010*, 48(4), 1088–1094

[29] BAE S., KIM H., LEE Y., XU X., PARK J.-S., ZHENG Y., BALAKRISHNAN J., LEI T., KIM H.R., SONG Y.I., KIM Y.-J., KIM K.S., ÖZYILMAZ B., AHN J.-H., HONG B.H., IIJIMA S.: Roll-to-roll production of 30-inch graphene films for transparent electrodes, Nat. Nanotech., *2010*, 5(8), 574–578

[30] LI X., MAGNUSON C.W., VENUGOPAL A., AN J., SUK J.W., HAN B., BORYSIAK M., CAI W., VELAMAKANNI A., ZHU Y., FU L., VOGEL E.M., VOELKL E., COLOMBO L., RUOFF R.S.: Graphene films with large domain size by a two-step chemical vapor deposition process, Nano Lett., *2010*, 10(1), 4328– 4334

[31] LI X., MAGNUSON C.W., VENUGOPAL A., TROMP R.M., HANNON J.B., VOGEL E.M., COLOMBO L., RUOFF R.S.: Large-area graphene single crystals grown by low-pressure chemical vapor deposition of methane on copper, J. Am. Chem. Soc., *2011*, 133(9), 2816–2819

[32] VLASSIOUK I., SMIRNOV S., SURWADE S.P., REGMI M., SRIVASTAVA N., FEENSTRA R., ERES GY., PARISH C., LAVRIK N., DATSKOS P., DAI S., FULVIO P.: Graphene nucleation density on copper: fundamental role of background pressure, J. Phys. Chem. C, *2013*, 117(37), 18919–18926

[33] BERGER C., SONG Z.M., LI X.B., WU X.S., BROWN N., NAUD C., MAYO D., LI T.B., HASS J., MARCHENKOV A.N, CONRAD E.H., FIRST P.N., DE HEER W.A.: Electronic confinement and coherence in patterned epitaxial graphene, Science, *2006*, 312(5777), 1191–1196

[34] BERGER C., SONG Z.M., LI T.B., LI X.B., OGBAZGHI A.Y., FENG R., DAI Z.T., MARCHENKOV A.N., CONRAD E.H., FIRST P.N., DE HEER W.A.: Ultrathin epitaxial graphite: 2D electron gas properties and a route toward graphene-based nanoelectronics, J. Phys. Chem. B, *2004*, 108(52), 19912–19916

[35] VLASSIOUK I., FULVIO P., MEYER H., LAVRIK N., DAI S., DATSKOS P., SMIRNOV S.: Large-scale atmospheric pressure chemical vapor deposition of graphene, Carbon, *2013*, 54(4), 58–67

[36] VAN GILS S., LE PEN C., HUBIN A., TERRYN H., STIJNSB E.: Electropolishing of copper in H₃PO₄ *ex situ* and *in situ* optical characterization, J. Electrochem. Soc., *2007*, 154(3), C175–C180

[37] SHIVAREDDY S., BAE S., BRANKOVIC S.: Cu surface morphology evolution during electropolishing, Electrochem. Solid State Lett., *2008*, 11(1), D13–D17

[38] WOOD J.D., SCHMUCKER S.W., LYONS A.S., POP E., LYDING J.W.: Effects of polycrystalline Cu substrate on graphene growth by chemical vapor deposition, Nano Lett., *2011*, 11(1), 4547–4554

[39] VLASSIOUK I., REGMI M., FULVIO P., DAI S., DATSKOS P., ERES G., SMIRNOV S.: Role of hydrogen in chemical vapor deposition growth of large single-crystal graphene, ACS Nano, *2011*, 5 (7), 6069–6076

[40] FLORES C.B., LÓPEZ D.M.: Multilayer graphene synthesized by CVD using liquid hexane as the carbon precursor, World J. Cond. Matter Phys., *2011*, 1(4), 157–160

[41] KIRKLAND N.T., SCHILLER T., MEDHEKAR N., BIRBILIS N.: Exploring graphene as a corrosion protection barrier, Corr. Sci., *2012*, 56(1), 1–4

[42] KOUSALYA A.S., KUMAR A., PAUL R., ZEMLYANOV D., FISHER T.S.: Graphene: An effective oxidation barrier coating for liquid and two-phase cooling systems, Corr. Sci., *2013*, 69(1), 5–10

[43] KALITA G., AYHAN M.E., SHARMA S., SHINDE S.M., GHIMIRE D., WAKITA K., UMENO M., TANEMURA M.: Low temperature deposited graphene by surface wave plasma CVD as effective oxidation resistive barrier, Corr. Sci., *2014*, 78(1), 183–187

[44] FRIEDRICH H., JACOBY G., MEISTER C.G.: Quantum reflection by Casimir–van der Waals potential tails, Phys. Rev. A, *2002*, 65(3), 032902–032915

[45] SUTTER E., ALBRECHT P., CAMINO F.E., SUTTER P.: Monolayer graphene as an ultimate chemical passivation layer for arbitrarily shaped metal surfaces, Carbon, *2010*, 48(15), 4414–4420

[46] SINGH RAMAN R.K., BANERJEE P.C., LOBO D.E., GULLAPALLI H., SUMANDASA M., KUMAR A., CHOUDHARY L., TKACZ R., AJAYAN P.M., MAJUMDER M.: Protecting copper from electrochemical degradation by graphene coating, Carbon, *2012*, 50(11), 4040–4045

[47] HSIEH Y.-P., HOFMANN M., CHANG K.-W., JHU J.G., LI Y.-Y., YAO CHEN K., YANG C.C., CHANG W.-S., CHEN L.-C.: Complete corrosion inhibition through graphene defect passivation, ACS Nano, *2014*, 8(1), 443–448

[48] HUH J.-H., KIM S.H., CHU J.H., KIM S.Y., KIM J.H., KWON S.-Y.: Enhancement of seawater corrosion resistance in copper using an acetone-derived graphene coating, Nanoscale, *2014*, 6(8), 4379–4386

[49] NAYAK P.K., HSU C.-J., WANG S.-C., J.C., SUNG HUANG J.-L.: Graphene coated Ni films: A protective coating, Thin Solid Films, *2013*, 529(1), 312–316

[50] XIA J., CHEN F., LI J., TAO N.: Measurement of the quantum capacitance of graphene, Nat. Nanotechnol., 2009, 4(8), 505–509

[51] WANG S., ZHANG L., XIA Z., ROY A., CHANG D.W., BAEK J.-B., DAI L.: BCN graphene as an efficient metal-free electrocatalyst for the oxygen reduction reaction, Angew. Chem. Int. Ed., *2012*, 51(17), 4209–4212

[52] ERNEST Y.: Dioxygen electrocatalysis: mechanism in relation to catalyst structure, J. Mol. Catal., *1986*, 38(1-2), 5–25

[53] SREEVATSA S., BANERJEE A., HAIM G.: Graphene as a permeable ionic barrier, ECS Trans., *2009*, 19(5), 259–264

[54] ROBINSON Z.R., TYAGI P., MURRAY T.M., VENTRICE C.A., CHEN S., MUNSON A., MAGNUSON C.W., RUOFF R.S.: Substrate grain size and orientation of Cu and Cu–Ni foils used for the growth of graphene films, J. Vac. Sci. Technol. A, Vac. Surf. Films, *2011*, 30(1), Art. No. 011401

[55] LI X., CAI W., COLOMBO L., RUOFF R.S.: Evolution of graphene growth on Ni and Cu by carbon isotope labeling, Nano Lett., *2009*, 9(12), 4268–4272

[56] SRIVASTAVA A., GALANDE C., CI L., SONG L., RAI C., JARIWALA D., KELLY K.F., AJAYAN P.M.: Multilayer graphene synthesized by CVD using liquid hexane as the carbon precursor, Chem. Mater., *2010*, 22(11), 3457–3461

[57] MIAO C., ZHENG C., LIANG O., XIE Y.-H.: Physics and applications of graphene - experiments, Ed. MIKHAILOV S., InTech Europe, Rijeka, Croatia, *2011*

[58] ZHOU X.: Graphene oxidation barrier coating, Ph.D. Thesis, University of Colorado, Boulder, CO USA, *2011*

[59] SCHRIVER M., REGAN W., GANNETT W.J., ZANIEWSKI A.M., CROMMIE M.F., ZETTL A.: Graphene as a long-term metal oxidation barrier: worse than nothing, ACS Nano, *2013*, 7(7), 5763–5768

[60] HADDAD F.S., THAKRAR R.R., HART A.J., SKINNER J.A., NARGOL A.V.F., NOLAN J.F., GILL H.S., MURRAY D.W., BLOM A.W., CASE C.P.: Metal-on-metal bearings, J. Bone Joint Surg. Br., *2011*, 93(B), 572–579

[61] KOROVESSIS P., PETSINIS G., REPANTI M., REPANTIS T.: Metallosis: After contemporary metal-on-metal total hip arthroplasty five to nine-year follow-up, J. Bone Joint Surg. Am., *2006*, 88(6), 1183–1191

[62] KAW M., SINGH S., GAGNEJA H., AZAD P.: Role of self-expandable metal stents in the palliation of malignant duodenal obstruction, Surg. Endosc., *2003*, 17(4), 646–650

[63] BARON T.H.: Expandable metal stents for the treatment of cancerous obstruction of the gastrointestinal tract, New Engl. J. Med., *2001*, 344(22), 1681–1687

[64] CORTIZO M., DEMELE M., CORTIZO A.: Metallic dental material biocompatibility in osteoblastlike cells, Biol. Trace Elem. Res., *2004*, 100(2), 151–168

[65] CRAIG R.G., POWERS J.M. (Eds.): Restorative dental materials, 11th Ed., Mosby Inc., St Louis, MO, USA, *2010*

[66] TONDATO F., NG D.W., SRIVATHSAN K., ALTEMOSE G.T., HALYARD M.Y., SCOTT L.R.: Radiotherapy-induced pacemaker and implantable cardioverter defibrillator malfunction, Expert Rev. Med. Dev., *2009*, 6(3), 243–249

[67] ISHII K., KODANI E., MIYAMOTO S., OTSUKA T., HOSONE M., OGATA K., SATO W., MATSUMOTO S., TADERA T. IBUKI KUSAMA Y., ATARASHI H.: Pacemaker Contact Dermatitis: The effective use of a polytetrafluoroethylene sheet, Pacing Clin. Electrophysiol., *2006*, 29(11), 1299–1302

[68] SCHMIDT C., IGNATIUS A.A., CLAES L.E.: Proliferation and differentiation parameters of human osteoblasts on titanium and steel surfaces, J. Biomed. Mater. Res., *2001*, 54(2), 209–215

[69] KURTZ S.M., MURATOGLU O.K., EVANS M., EDIDIN A.A.: Advances in the processing, sterilization, and crosslinking of ultra-high molecular weight polyethylene for total joint arthroplasty, Biomaterials, *1999*, 20(18) 1659–1688

[70] DAVIS J.R.: Handbook of materials for medical devices, First Ed., ASM International, Materials Park, OH, USA, *2003*

[71] ATWOOD R.C., LEE P.D., CURTIS R.V.: Modeling the surface contamination of dental titanium investment castings, Dent. Mater., *2005*, 21(2), 178–186

[72] CAICEDO M.S., PENNEKAMP P.H., MCALLISTER K., JACOBS J.J., HALLAB N.J.: Soluble ions more than particulate cobalt-alloy implant debris induce monocyte costimulatory molecule expression and release of proin flammatory cytokines critical to metal-induced lymphocyte reactivity, J. Biomed. Mater. Res., *2010*, A93A(4), 1312–1321

[73] ROMESBURG J.W., WASSERMAN P.L., SCHOPPE C.H.: Metallosis and Metal-Induced Synovitis Following Total Knee Arthroplasty, Rev. Radiograp. CT Findings, *2010*, 4(9), 7–17

[74] JACOBS J.J., HALLAB N.J.: Loosening and osteolysis associated with metal-on-metal bearings: A local effect of metal hypersensitivity?, J. Bone Joint Surg. Am., *2006*, 88(6), 1171–1172

[75] YANG L., SHELDON B.W., WEBSTER T.J.: Orthopedic nano diamond coatings: Control of surface properties and their impact on osteoblast adhesion and proliferation, J. Biomed. Mater. Res., *2009*, A91A(2), 548–556

[76] PECHEVA E., PRAMATAROVA L., FINGAROVA D., HIKOV T., DINEVA I., KARAGYOZOVA Z., STAVREV S.: Advanced materials for metal implant coatings, J. Optoelectron. Adv. Mater., *2009*, 11(9), 1323–1326

[77] PODILA R., MOORE T., ALEXIS F., RAO A.M.: Graphene coatings for enhanced hemo-compatibility of nitinol stents, Rev. Soc. Chem. Adv., *2013*, 3(1), 1660–1665

[78] PODILA R., MOORE T., ALEXIS F.R.: Graphene coatings for biomedical implants, J. Vis. Exp., *2013*, 73(1), Art. No. e50276

[79] ZHANG W., LEE S., MCNEAR K.L., CHUNG T.F., LEE S., LEE K., CRIST S.A., RATLIFF T.L., ZHONG Z. YANG C.: Use of graphene as a protection film in biological environments, Sci. Rep. *2014*, 4(4), 4097

[80] NEUHAUSER E.F., LOEHR R.C., MILLIGAN D.L., MALECKI M.R.: Toxicity of metals to the earthworm *Eisenia fetida*, Biol. Fert. Soils, *1985*, 1(3), 149–152

[81] KOENIG S.P., BODDETI N.G., DUNN M.L., BUNCH J.S.: Ultrastrong adhesion of graphene membranes, Nat. Nano., 2011, 6(9), 543–546

[82] CAPRIOLI F., DECKER F., MARRANI A.G., BECCARI M., CASTRO V.D.: Copper protection by self-assembled monolayers of aromatic thiols in alkaline solutions, Phys. Chem. Chem. Phys., *2010*, 12(32), 9230–9238

[83] LUSK A.T., JENNINGS G.K.: Characterization of self-assembled monolayers formed from sodium s-alkyl thiosulfates on copper, Langmuir, *2001*, 17(25), 7830–7836

[84] BRINKER C.J., HURD A.J., SHUNK P.R., FRYE G.C., ASHLEY C.S.: Review of sol-gel thin film formation, J. Non-Cryst. Solids, *1992*, 147-148(1), 424–436

[85] SCRIVEN L.E.: in Better Ceramics through Chemistry III, Eds., BRINKER C.J., CLARK D.E., ULRICH D.R., The Materials Research Society, Pittsburgh, PA USA, *1988*, p.717

[86] LANDAU L.D., LEVICH B.G.: Dragging of a liquid by a moving plate, Acta Physiochim. U.R.S.S., *1942*, 17, 42–54

[87] DISLICH H.: Sol-gel: science, processes and products, J. Non-Cryst. Solids, *1997*, 80(1-3), 115–121

[88] ARFSTEN N.J., ERBLE A., OTTO J., REICH A.: Investigations on the angle-dependent dip coating technique, ADDC, for the for the Production of Optical Filters, J. Sol-Gel Sci. Techol., *1997*, 8(1-3), 1099–1104

[89] SCHMIDT H., in Chemistry, Spectroscopy and Application of sol-gel glasses, Ed., REISFELD R. Springer-Verlag, Berlin, Germany, *1992*, pp.119–152

[90] MEYERHOFER D.: Characteristics of resist films produced by spinning, J. Appl. Phys., *1978*, 49(7), 3993–3997

[91] LAI J.H.: An investigation of spin coating of electron resists, Polym. Eng. Sci., *1979*, 19(15), 1117–1121

[92] CHEN B.T.: Investigation of the solvent-evaporation effect on spin coating of thin films, Polym. Eng. Sci., *1983*, 23(7), 399–403

[93] VAN BOMMEL J.: Optical coatings for computer monitors and TV screens, Glass Res., *1997*, 10, 7

[94] O'BRIEN S.B.G., SCHWARTZ L.W.: Theory and modeling of thin film flows, Encyclopedia of Surface and Colloid Science, Ed. HUBBARD A., Marcel Dekker, New York, *2002*, pp. 5283–5297

[95] EVANS P.L., SCHWARTZ L.W., ROY R.V.: Three-dimensional solutions for coating flow on a rotating horizontal cylinder: Theory and experiment, Phys. Fluids, *2005*, 17(7), Art. No. 072102

[96] FLOCH H.G., BELLEVILLE G., PRIOTTON J.J.: Sol-Gel Optical Coatings For Lasers., Am. Ceram. Soc. Bull., *1995*, 74(10), 60–63

[97] FLOCH H.G., BELLEVILLE P.F.: Scratch-Resistant Single-Layer Antireflective Coating By A Low Temperature Sol-Gel Route, Proc. Spie, *1992*, 1758, 135–149

[98] MITSOULIS E., ATHANASOPOULOS G.: Numerical Simulation Of Blade-Over-Roll Coating Forming Flows, Comp. Met. Mater., *2010*, 10(4), 214–224

[99] NODA K., YAMAGAMI YAMAMOTO M., M., SATO H., ITAYA H., OKAJIMA A., YAMADA M.: Thin Film Formation By Direct Reverse Roll-Coating On Plastic Web, Jpn. J. Appl. Phys., *2003*, 42(1), 5722–5725

[100] ALONSO S., REÂGLAT O., BERTRAND F., CHOPLIN L., TANGUY P.A.: Process viscosity in reverse roll coating, Trans. I. Chem. E, *2001*, 79(Part A), 128–136

[101] EMSLIE A.G., BONNER F.T., PECK C.G.: Flow of a viscous liquid on a rotating disk, J. Appl. Phys., *1958*, 29(5), 858–862

[102] ACRIVOS A., SHAH M.J., PETERSEN E.E.: On the flow of a non-Newtonian liquid on a rotating disk, J. Appl. Phys., *1960*, 31(6), 963–968

[103] KIM D.-Y., SINHA-RAY S., PARK J.-J., LEE J.-G., CHA Y.-H., BAE S.-H., AHN J.-H., JUNG Y.C., KIM S.M., YARIN A.L., YOON S.S.: Self-healing reduced graphene oxide films by supersonic kinetic spraying, Adv. Funct. Mater. *2014*, 24(31), 4986–4995

[104] WANG S.J., GENG Y., ZHENG Q., KIM J.-K.: Fabrication of highly conducting and transparent graphene films, Carbon, *2010*, 48(6), 1815–1823

[105] YOON S., KIM H.J., LEE C.: Fabrication of an automotive heat exchanger using a kinetic spraying process, Surf. Coat. Technol., *2007*, 201(1) 9524–9532

[106] DZHURINSKIY D., MAEVA E., LESHCHINSKY EV., MAEV, R.GR.: Corrosion Protection of Light Alloys Using Low Pressure Cold Spray, J. Therm. Spray Technol., *2012*, 21(2) 304–313

[107] HUSSAIN T., MCCARTNEY D.G., SHIPWAY P.H., MARROCCO T.: Corrosion behavior of cold sprayed titanium coatings and free standing deposits, J. Therm. Spray Technol., *2011*, 20(1-2), 260–274

[108] YARIN A.L., KOOMBHONGSE S., RENEKER D.H.: Taylor cone and jetting from liquid droplets in the electrospinning of nanofibers, J. Appl. Phys., *2001*, 90(9), 4836–4846

[109] SHIN Y.M., HOHMAN M.M., BRENNER M.P., RUTLEDGE G.C.: Experimental characterization of electrospinning: the electrically forced jet and instabilities, Polymer, *2001*, 42(25), 9955–9967

[110] MENCHACA C., MANOUN B., MARTÍNEZ-BARRERA G., CASTANO V.M., LÓPEZ-VALDIVIA H.: In situ high-temperature Raman study of crystalline nylon 6,12 fibers gamma-irradiated in an argon atmosphere, J. Phys. Chem. Solids, *2006*, 67 (9), 2111–2118

[111] CAMPOS C.M., PÉREZ C.G., CASTAÑEDA I., GARCÍA-SÁNCHEZ M.A., GUARDIÁN R., URUCHURTU J.: Nylon/graphene oxideelectrospun composite coating, Internat. J. Polym. Sci., *2013*, 1, 1-9

[112] KAYA C.: Al$_2$O$_3$-Y-TZP/Al$_2$O$_3$ functionally graded composites of tubular shape from nano-sols using double-step electrophoretic deposition, J. Eur. Ceram. Soc., *2003*, 23(10), 1655–1660

[113] PUT S., VLEUGELS J., VAN DER BIEST O.: Functionally graded WC–co materials produced by electrophoretic deposition, Scr. Mater., *2001*, 45(10), 1139–1145

[114] SARKAR P., DATTA S., NICHOLSON P.S.: Functionally graded ceramic/ceramic and metal/ceramic composites by electrophoretic deposition, Compos. B-Eng., *1997*, 28(1), 49–56

[115] LEE S.B., CHOI O., LEE W., YI J.W., KIM B.S., BYUN J.H., YOON M.K., FONG H., THOSTENSON E.T., CHOU T.W.: Processing and characterization of multi-scale hybrid composites reinforced with nanoscale carbon reinforcements and carbon fibers, Compos. Part A, *2001*, 42(4), 337–344

[116] ZHITOMIRSKY I.: Hydroxyapatite coatings and fibers, Mater. Lett., *2000*, 42, 262

[117] YOU C., JIANG D.L., JAN S.H.: SiC/TiC laminated structure shaped by electrophoretic deposition, Ceram. Int., *2004*, 30(5), 813–815

[118] VAN DE PERRE L., VAN DER BIEST O.: Composite SiC-graphite interlayers for crack deflection in ceramic laminates, Silic. Ind., *1998*, 63, 39–43

[119] KAYA C., KAYA F., SU B., THOMAS B., BOCCACCINI A.R.: Structural and functional thick ceramic coatings by electrophoretic deposition, Surf. Coat. Technol., *2005*, 191(1), 303–310

[120] YANAGIDA A., NAKAJIMA Y., KAMESHIMA N., YOSHIDA T., WATANABE K., OKADA K.: Preparation of a crack-free rough titania coating on a stainless steel mesh by electrophoretic deposition, Mater. Res. Bull., *2005*, 40(1), 1335–1344

[121] PEIRO A.M., BRILLA E., PERAL J., DOMENECH X., AYLLON J.A.: Electrochemically assisted deposition of titanium dioxide on aluminium cathodes, J.Mater.Chem., *2002*, 12(1), 2769–2773

[122] BOCCACCINI A.R., ROETHER J.A., THOMAS B.J.C., SHAFFER M.S.P., CHAVEZ E., STOLL E., MINAY E.J.: 'The electrophoretic deposition of inorganic nanoscaled materials, J. Ceram. Soc. Jpn., *2006*, 114(1325), 1–14

[123] BESRA L., LIU M.: A review on fundamentals and applications of electrophoretic deposition number , EPD , Prog. Mater. Sci., *2007*, 52, 1

[124] VU Q.-T., PAVLIK M., HEBESTREIT N., PFLEGER J., RAMMELT U., PLIETH W.: Electrophoretic deposition of nanocomposites formed from polythiophene and metal oxides, Electrochim. Acta, *2005*, 51(6), 1117–1124

[125] PECH-RODRÍGUEZ W.J., GONZÁLEZ-QUIJANO D., VARGAS-GUTIÉRREZ G., RODRÍGUEZ-VARELA F.J.: Deposition of Vulcan XC-72 coatings on stainless steel bipolar plates by reverse pulsed dc voltage electrophoretic deposition number, EPD, for fuel cell applications, ECS Trans., *2014*, 58(12), 33–39

[126] LIH E.T.Y., ZAID R.T.M., LING T.L., CHONG K.F.: Facile corrosion protection coating from graphene, Int. J. Chem. Engin. Appl., *2012*, 3(6), 453–455

[127] SINGH B.P., NAYAK S., NANDA K.K., JENA B.K., BHATTACHARJEE S., BESRA L.: The production of a corrosion resistant graphene reinforced composite coating on copper by electrophoretic deposition, Carbon, *2013*, 61(1), 47–56

[128] HE W., ZHU L., CHEN H., NAN H., LI W., LIU H., WANG Y.: Electrophoretic deposition of graphene oxide as a corrosion inhibitor for sintered NdFeB, Appl. Surf. Sci., *2013*, 279(1), 416–423

[129] KOLBE H.: Decomposition of valeric acid by an electric current, Annal. Chem. Pharm., *1848*, 64(1), 339–341 (in German)

[130] KOLBE H.: Studies of the electrolysis of organic compounds, Annal. Chem. Pharm., *1849*, 69(1), 257–294 (in German)

[131] SINGH B.P., JENA B.K., BHATTACHARJEE S., BESRA L.: Development of the oxidation and corrosion resistanr hydrophobic graphene oxide-polymer composite coating on copper, Surf. Coat. Technol., *2013*, 232(1), 475–481

[132] WANG M., DUONG L.D., OH J.-S., MAI N.T., KIM S., HONG S., WANG T.H., LEE Y.K., NAM J.-D.: Large-Area, conductive and flexible reduced graphene oxide number, RGO, membrane fabricated by electrophoretic deposition number, EPD, ACS Appl. Mater. Interfaces, *2014*, 6(3), 1747–1753

[133] MEYERS J.P., DARLING R.M.: Model of carbon corrosion in PEM fuel cells, J. Electrochem. Soc., *2006*, 153(8), A1432–A1442

[134] PRABAKAR S.J.R., HWANG Y.-H., BAE E.G., LEE D.K., PYO M.: Graphene oxide as a corrosion inhibitor for the aluminium current collector in lithium ion batteries, Carbon, *2013*, 52(1), 128–136

[135] LOGAN B.E., HAMELERS B., ROZENDAL R., SCHRÖDER U., KELLER J., FREGUIA S., AELTERMAN P., VERSTRAETE W., RABAEY K.: Microbial fuel cells: methodology and technology, Environ. Sci. Technol., *2006*, 40(17), 5181–5192

[136] KRISHNAMURTHY A., GADHAMSHETTY V., MUKHERJEE R., CHEN Z., REN W., CHENG H-M., KORATKAR N.: Passivation of microbial corrosion using a graphene coating, Carbon, *2013*, 56(1), 45–49

[137] SAHU S.C., SAMANTARA A.K., SETH M., PARWAIZ S., SINGH B.P., RATH P.C., JENA B.K.: A facile electrochemical approach for the development of highly corrosion protective coatings using graphene nanosheets, Electrochem. Commun., *2013*, 32(1), 22–26

[138] WESSLING B.: Passivation of metals by coating with polyaniline: Corrosion potential shift and morphological changes, Adv. Mater., *1994*, 6(3), 226–228

[139] DEBERRY D.W.: Modification of the electrochemical and corrosion behavior of stainless steels with an electroactive coating, J. Electrochem. Soc., *1985*, 132(5), 1022–1026

[140] WEI Y., WANG J., JIA X., YEH J.M., SPELLANE P.: Polyaniline as corrosion protection coatings on cold rolled steel, Polymer, *1995*, 36(23), 4535–4537

[141] YEH J.M., LIOU S.J., LAI C.Y., WU P.C., TSAI T.Y.: Enhancement of the corrosion protection effect in polyaniline *via* the formation of polyaniline-clay nanocomposite materials, Chem. Mater., *2001*, 13(3), 1131–1136

[142] IONITA M., PRUNA A.: Polypyrrole/carbon nanotube composites: Molecular modeling and experimental investigation as an anti-corrosive coating, Prog. Org. Coat., *2011*, 72(4), 647–652

[143] MARTINA V., DE RICCARDIS M.F., CARBONE D., ROTOLO P., BOZZINI B., MELE C.: Electrodeposition of polyaniline–carbon nanotubes composite films and investigation on their role in corrosion protection of austenitic stainless steel by SNIFTIR analysis: J. Nanopart. Res., *2011*, 13(11), 6035–6047

[144] SALAM M.A., AL-JUAID S.S., QUSTI A.H., HERMAS A.A.: Electrochemical deposition of a carbon nanotube-poly o-phenylenediamine, composite on a stainless steel surface, Synth. Met., *2011*, 161(1-2), 153–157

[145] HU S.T., KONG X.H., YANG H., SUN R.H.: Anticorrosive films prepared by incorporating permanganate modified carbon nanotubes into the waterborne polyurethane polymer, Adv. Mater. Res., *2011*, 189–193, 1157–1162

[146] DE RICCARDIS M.F., MARTINA V., CARBONE D., ROTOLO P.: Functional characterisations of hybrid nanocomposite films based on polyaniline and carbon nanotubes, Adv. Sci. Technol., *2013*, 79(1), 81–86

[147] GERGELY A., PÁSZTI Z., MIHÁLY J., DROTÁR E., TÖRÖK T.: Galvanic corrosion prevention of the zinc-rich hybrid coatings facilitated by the percolating structure of the carbon nanotubes Part II: Protection properties and mechanism of the hybrid coatings, Prog. Org. Coat., *2014*, 77(2), 412–424

[148] GERGELY A., PÁSZTI Z., HAKKEL O., MIHÁLY J., KÁLMÁN E.: Corrosion protection of cold-rolled steel with alkyd paint coatings composited with various microstructure arranged polypyrrole-modified nano-size alumina and carbon nanotubes, Mater. Sci. Eng. B, *2012*, 177(18), 1571–1682

[149] GERGELY A., PÁSZTI Z., HAKKEL O., BERTÓTI I., MIHÁLY J., TÖRÖK T.: Investigation of modified carbon nanotubes/aluminium-oxide monohydrate containing zinc-rich hybrid paint coatings, Korr. Figy., *2013*, 53(1), 3–24 (in Hungarian)

[150] GERGELY A., TÖRÖK T.: Optimally balanced active-passive corrosion protection by zinc-rich paint coatings featuring proper hybrid formulation with polypyrrole modified carbon nanotubes, Mater. Sci. For., *2013*, 752(1), 275–283

[151] GERGELY A., PÁSZTI Z., BERTÓTI I., TÖRÖK T., MIHÁLY J., KÁLMÁN E.: Novel zinc-rich epoxy paint coatings with hydrated alumina and carbon nanotubes supported polypyrrole for corrosion protection of low carbon steel Part II: Corrosion prevention behaviour of the hybrid paint coatings, Mater. Corr., *2013*, 64(12), 1091–1103

[152] GERGELY A., TÖRÖK T., PÁSZTI Z., BERTÓTI I., MIHÁLY J., KÁLMÁN E.: Zinc-rich paint coatings containing either ionic surfactant-modified or functionalized multi-walled carbon nanotube-supported polypyrrole utilized to protect cold-rolled steel against corrosion, Nova Science Publishers, Inc., Part II: Application of Carbon nanotubes, *2012*, Chapter 10th, pp. 211–258.

[153] JEON H., PARK J., SHON M.: Corrosion protection by epoxy coating containing multi-walled carbon nanotubes, J. Ind. Engin. Chem., *2013*, 19(3), 849–853

[154] SHOW Y., NAKASHIMA T., FUKAMI Y.: Anticorrosion coating of carbon nanotube/polytetra-fluoroethylene composite film on the stainless steel bipolar plate for proton exchange membrane fuel cells, J. Nanomater., *2013*, Article ID 378752

[155] DESHPANDE P.P., VATHARE S.S., VAGGE S.T., TOMŠÍK E., STEJSKAL J.: Conducting polyaniline/multi-wall carbon nanotubes composite paints on low carbon steel for corrosion protection: Electro-chemical investigations, Chem. Pap., *2013*, 67(8), 1072–1078

[156] SREEVATSA S.: Carbon nanotube electronic structures as anti-corrosion coatings, PhD Thesis, State University of New Jersey, Newark, USA, 2009

[157] PRAVEEN B.M., VENKATESHA T.V., ARTHOBA NAIK Y., PRASHANTHA K.: Corrosion studies of carbon nanotubes–Zn composite coating, Surf. Coat. Technol., *2007*, 201(12), 5836–5842

[158] CHEN X.H., CHEN C.S., XIAO H.N., CHENG F.Q., ZHANG G., YI G.J.: Corrosion behavior of carbon nanotubes–Ni composite coating, Surf. Coat. Technol., *2005*, 191(2-3), 351–356

[159] MONTEMOR M.F., FERREIRA M.G.S.: Analytical characterisation and corrosion behaviour of bis-aminosilane coatings modified with carbon nanotubes activated with rare-earth salts applied on AZ31 Magnesium alloy, Surf. Coat. Technol., *2008*, 202(19), 4766–4774

[160] RAFIEE M.A., RAFIEE J., WANG Z., SONG H., YU Z.Z., KORATKAR N.: Enhanced mechanical properties of nanocomposites of low graphene content, ACS Nano, *2009*, 3(12), 3884–3890

[161] ZHANG W.L., LIU Y.D., CHOI H.J.: Fabrication of semiconducting graphene oxide/polyaniline composite particles and their electrorheological response under an applied electric field, Carbon, *2012*, 50(1), 290–296

[162] ZHANG W.L., PARK B.J., CHOI H.J.: Colloidal graphene oxide/polyaniline nanocomposite and its electrorheology, Chem. Commun., *2010*, 46(30), 5596–5598

[163] STANKOVICH S., PINER R.D., NGUYEN S.T., RUOFF R.S.: Synthesis and exfoliation of isocyanate-treated graphene oxide nanoplatelets, Carbon, *2006*, 44(15), 3342–3347

[164] COMPTON O.C., KIM S., PIERRE C., TORKELSON J.M., NGUYEN S.T.: Crumpled graphene nanosheets as highly effective barrier property enhancers, Adv. Mater., *2010*, 22(42), 4759–4763

[165] KIM H.W., MIURA Y., MACOSKO C.W.: Graphene/polyurethane composites for improved gas barrier and electrical conductivity, Chem. Mater., *2010*, 22(11), 3441–3450

[166] KIM H.W., MACOSKO C.W.: Dispersing organoclay in polystyrene melts: roles of stress and diffusion, Macromolecules, *2008*, 41(9), 3317–3327

[167] KALAITZIDOU K., FUKUSHIMA H., DRZAL L.T.: Multifunctional polypropylene composites produced by the incorporation of exfoliated graphite nanoplatelets, Carbon, *2007*, 45(7), 1446–1452

[168] KIM H.W., ABDALA A.A., MACOSKO C.W.: Graphene/polymer composites, Macromolecules, *2010*, 43(16), 6515–6530

[169] POTTS J.R., DREYER D.R., BIELAWSKI C.W., RUOFF R.S.: Graphene-based polymer composites, Polymer, *2011*, 52(1), 5–25

[170] CHANG C.-H., HUANG T.-C., PENG C.-W., YEH T.-C., LU H.-I., HUNG W.-I., WENG C.-J., YANG T.-I., YEH J.-M.: Novel anticorrosion coatings prepared from polyaniline/graphene composites, Carbon, *2012*, 50(14), 5044–5051

[171] LIU T., YIN Y., CHEN S., CHANG X., CHENG S.: Super-hydrophobic surfaces improve corrosion resistance of copper in seawater, Electrochim. Acta, *2007*, 52(11), 3709–3882

[172] ZHANG F., ZHAO L., CHEN H., XU S., EVANS D.G., DUAN X.: Corrosion resistance of superhydrophobic layered double hydroxide films on aluminium, Angew. Chem. Int. Ed., *2008*, 47(13), 2466–2469

[173] ZHANG F., CHEN S., DONG L., LEI Y., LIU T., Y.YIN: Preparation of superhydrophobic films on titanium as effective corrosion barriers, Appl. Surf. Sci., *2011*, 257(7), 2587–2591

[174] RAO A.V., LATTHE S., MAHADIK S., KAPPENSTEIN C.: Mechanically stable and corrosion resistant superhydrophobic sol–gel coatings on copper substrate, Appl. Surf. Sci., *2011*, 257(13), 5772–5776

[175] WENG C.J., CHANG C.H., PENG C.W., CHEN S.W., YEH J.M., HSU C.L., WEI Y.: Advanced anticorrosive coatings prepared from the mimicked Xanthosomasagittifolium leaf-like electroactive epoxy with synergistic effects of superhydrophobicity and redox catalytic capability, Chem. Mater., *2011*, 23(8), 2075–2083

[176] YANG T.I., PENG C.W., LIN Y.L., WENG C.J., EDGINGTON G., MYLONAKIS A., HUANG T.-C., HSU C.-H., YEH J.-M., WEI Y.: Synergistic effect of electroactivity and hydrophobicity on the anticorrosion property of room-temperature-cured epoxy coatings with multi-scale structures mimicking the surface of Xanthosomasagittifolium leaf, J. Mater. Chem., *2012*, 22(31), 15845–15852

[177] HIL R., MA M.: Superhydrophobic surfaces, Curr. Opin. Colloid Interface Sci., *2006*, 11(4), 193–202

[178] CHANG K.-C., HSU M.-H., LU H.-I., LAI M.-C., P LIU.-J., HSU C.-H., JI W.-F., CHUANG T.-L., WEI Y., YEH J.-M., LIU W.-R.: Room-temperature cured hydrophobic epoxy/graphene composites as a corrosion inhibitor for cold-rolled steel, Carbon, *2014*, 66(1), 144–153

[179] TURHAN M.C., LI Q., JHA H., SINGER R.F., VIRTANEN S.: Corrosion behaviour of multiwall carbon nanotube/magnesium composites in 3.5% NaCl, Electrochim. Acta, *2011*, 56(20), 7141–7148

[180] LI Q., TURHAN M.C., ROTTMAIR C.A., SINGER R.F., VIRTANEN S.: Influence of MWCNT dispersion on the corrosion behaviour of their Mg composites, Mater. Corr., *2012*, 63(5), 384–387

[181] FUKUDA H., SZPUNAR J.A., KONDOH K., CHROMIK R.: The influence of carbon nanotubes on the corrosion behaviour of AZ31B magnesium alloy, Corr. Sci., *2010*, 52(12), 3917–3923

[182] AUNG N.N., ZHOU W., GOH C.S., MUI S., NAI L., WEI J.: Effect of carbon nanotubes on the corrosion of Mg–CNT composites, Corr. Sci., *2010*, 52(5), 1551–1553

[183] ZHANG M., YAN Y., GONG K., MAO L., GUO Z., CHEN Y.: Electrostatic layer by layer assembled carbon nanotube mutilayer film and its catalytic activity for the oxygen reduction reaction, Langmuir, *2004*, 20(20), 8781–8785

[184] JÜRMANN G., TAMMEVESKI K.: Electroreduction of oxygen on multi-walled carbon nanotube modified highly oriented pyrolytic graphite electrodes in an alkaline solution, J. Electroanal. Chem., *2006*, 597(2), 119–126

[185] WANG S., IYYAMPERUMAL E., ROY A., XUE Y., YU D., DAI L.: Vertically aligned BCN nanotubes as efficient metal-free electrocatalysts for the oxygen reduction reaction: A synergetic effect by co-doping with boron and nitrogen, Angew. Chem., *2011*, 123(49), 11960–11964

[186] KUMAR C.M.P., VENKATESHA T.V., SHABADI R.: Preparation and corrosion behavior of Ni and Ni–graphene composite coatings, Mater. Res. Bull., *2013*, 48(4), 1477–1483

[187] DENNIS R.V., VIYANNALAGE L.T., GAIKWAD A.V., ROUT T.K., BANERJEE S.: Graphene nanocomposite coatings for protecting low-alloy steels from corrosion, Am. Ceram. Soc. Bull., *2013*, 92(5), 18–24

[188] ROUT T.K., GAIKWAD A.V., DINGEMANS T.A.: A method of preparing a polyetherimide coating on a metallic substrate, World Intellectual Property Organization, Pat. No. WO2011035920, A1, *2011*

[189] ROUT G.K., GAIKWAD A.V., LEE V., BANERJEE S.: Hybrid nanocomposite coatings for corrosion protection of low carbon steel: A substrate-integrated and scalable active–passive approach, J. Mater. Res., *2011*, 26(6), 837–844

[190] ROUT T.K., JHA G., SINGH A.K., BANDYOPADHYAY N., MOHANTY O.N.: Development of conducting polyaniline coating: A novel approach to superior corrosion resistance, Surf. Coat. Technol., *2003*, 67(1), 16–24

[191] KUMAR S., SUN L.L., CACERES S., LI B., WOOD W., PERUGINI A., MAGUIRE R.G., ZHONG W.H.: Dynamic synergy of graphitic nanoplatelets and multi-walled carbon nanotubes in polyetherimide nanocomposites, Nanotechnology, *2010*, 21(10), 105702–105710

[192] WILSON D., STENZENBERGER H.D., HERGENROTHER P.M.: Polyimides, Chapman and Hall, London, U.K., *1990*

[193] KUMAR S., LI B., CACERES S., MAGUIRE R.G., ZHONG W.-H.: Dramatic property enhancement in polyetherimide using low-cost commercially functionalized multi-walled carbon nanotubes *via* a facile solution processing method, Nanotech., *2009*, 20(46), 465708–465716

[194] VON BAECKMANN W., SCHWENK W., PRINZ W. (Eds.): Handbook of corrosion protection, Theory and practice of electrochemical protection processes, Third Edition, Golf Publishing Company, Houston TX, USA, *1997*